Article

Cell

The Root Cap Cuticle: A Cell Wall Structure for Seedling Establishment and Lateral Root Formation

Graphical Abstract

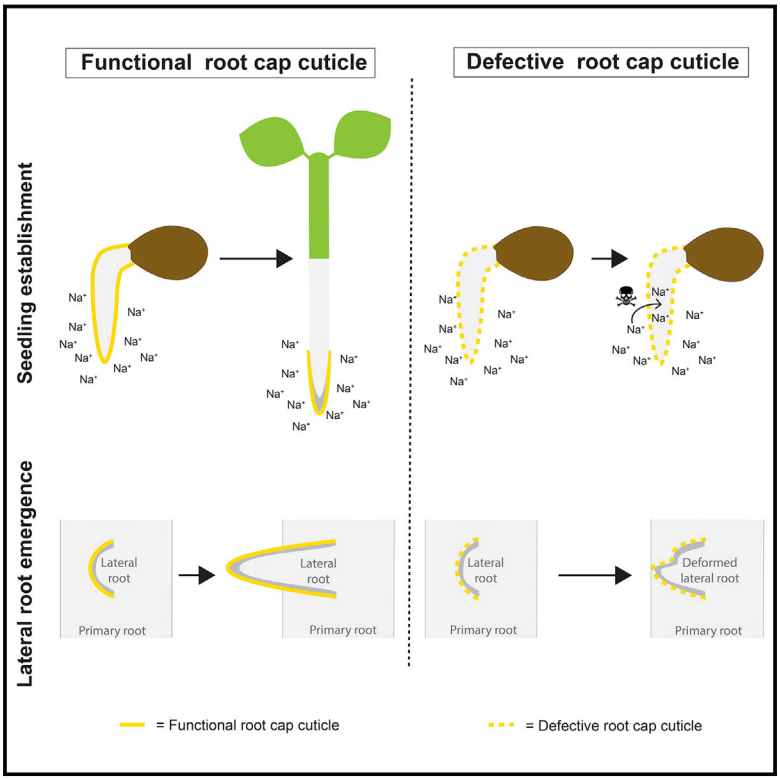

Authors

Alice Berhin, Damien de Bellis, Rochus B. Franke, Rafael A. Buono, Moritz K. Nowack, Christiane Nawrath

Correspondence

christiane.nawrath@unil.ch

In Brief

A cuticle-like cell wall structure on plant root caps protects seedlings from abiotic stress and contributes to proper lateral root outgrowth.

Highlights

- At early developmental stages, root caps of primary and lateral roots form a cuticle
- This polyester-rich cuticle is lost with the removal of the first root cap cell layer
- During germination, the root cap cuticle protects the sensitive root meristem
- The cuticle of young lateral roots facilitates invasive growth and root emergence

Berhin et al., 2019, Cell *176*, 1367–1378
March 7, 2019
https://doi.org/10.1016/j.cell.2019.01.005

CellPress

Article

Cell

The Root Cap Cuticle: A Cell Wall Structure for Seedling Establishment and Lateral Root Formation

Alice Berhin,[1] Damien de Bellis,[1,2] Rochus B. Franke,[3] Rafael A. Buono,[4,5] Moritz K. Nowack,[4,5] and Christiane Nawrath[1,6,*]

[1]Department of Plant Molecular Biology, University of Lausanne, Biophore Building, 1015 Lausanne, Switzerland
[2]Electron Microscopy Facility, University of Lausanne, Biophore Building, 1015 Lausanne, Switzerland
[3]Institute of Cellular and Molecular Botany, University of Bonn, Kirschallee 1, 53115 Bonn, Germany
[4]Department of Plant Biotechnology and Bioinformatics, Ghent University, Technologiepark 71, 9052 Ghent, Belgium
[5]VIB Center for Plant Systems Biology, Technologiepark 71, 9052 Ghent, Belgium
[6]Lead Contact
*Correspondence: christiane.nawrath@unil.ch
https://doi.org/10.1016/j.cell.2019.01.005

SUMMARY

The root cap surrounding the tip of plant roots is thought to protect the delicate stem cells in the root meristem. We discovered that the first layer of root cap cells is covered by an electron-opaque cell wall modification resembling a plant cuticle. Cuticles are polyester-based protective structures considered exclusive to aerial plant organs. Mutations in cutin biosynthesis genes affect the composition and ultrastructure of this cuticular structure, confirming its cutin-like characteristics. Strikingly, targeted degradation of the root cap cuticle causes a hypersensitivity to abiotic stresses during seedling establishment. Furthermore, lateral root primordia also display a cuticle that, when defective, causes delayed outgrowth and organ deformations, suggesting that it facilitates lateral root emergence. Our results show that the previously unrecognized root cap cuticle protects the root meristem during the critical phase of seedling establishment and promotes the efficient formation of lateral roots.

INTRODUCTION

Higher organisms adapted to the life on land by developing surface modifications protecting themselves against desiccation and other environmental stresses, including pathogen attack. In contrast to animals that incorporate specialized proteins in the extracellular matrix of the skin (Alberts et al., 2015), plants developed lipid-derived modifications on the surface of different organs (Kolattukudy, 2001a; Pollard et al., 2008). Aerial organs of the shoot that are in primary growth stage, such as leaves, flowers, and fruits have acquired a cuticle (Riederer, 2006). The cuticle forms a multi-layered structure of lipid components at the outermost surface of the organ in continuation with the cell wall (Jeffree, 2006). In most species, the main components of the cuticle are an insoluble structural polyester, named cutin, and a mixture of solvent-extractable compounds, commonly called waxes (Holloway, 1982a; Kolattukudy, 1980). Inner border tissues, organs in secondary growth stage, and wounded tissues are protected by lamellae containing suberin, a polymer similar to cutin but with higher amounts of phenolic compounds (Andersen et al., 2015; Franke et al., 2012; Pollard et al., 2008). Importantly, in contrast to cutin, which is primarily deposited on the outermost surface of the cell wall, suberin is formed as part of the secondary cell wall, deposited between the primary wall and the plasma membrane (Kolattukudy, 2001b; Pollard et al., 2008, Nawrath et al., 2013). Other plant organs are protected by specialized lipid-derived cell wall modifications, such as pollen containing sporopollenin and seeds forming seed coats containing suberin (Dominguez et al., 1999; Molina et al., 2006).

The cuticle that is synthesized by the epidermis of the shoot varies strongly in composition, architecture, and properties depending on the species, organ, and developmental stage as well as environmental conditions (Jeffree, 2006). Despite of being a surface structure with diffusion barrier properties, the cuticle has multiple functions beyond plant protection against water loss and abiotic stresses, such as in plant development preventing organ adhesions and fusions (Ingram and Nawrath, 2017; Nawrath et al., 2013). A cuticle can already be identified during early embryogenesis at globular stage when the embryo consists of a few dozen cells (Szczuka and Szczuka, 2003). From this stage on, it continuously expands with the growth of the plant. The cuticle of the embryo has also multiple functions in plant development, for example it plays a role in the establishment of identity of the epidermis of the shoot, in addition to preventing adhesions between embryo and maternal tissues (Ingram and Nawrath, 2017).

The polyester cutin consists predominantly of C16 and C18 oxygenated fatty acids, such as hydroxylated fatty acids and dicarboxylic acids, as well as glycerol. The interconnectivity between the monomers determines the polymer structure and its properties (Bakan and Marion, 2017; Yang et al., 2016). The biosynthesis of cutin comprises the formation of precursors within the cell, their export and the assembly of the polyester

within the cuticle (Fich et al., 2016; Nawrath et al., 2013). A key step of precursor formation is the synthesis of *sn-2*-monoacylglycerols from CoA-activated oxygenated fatty acids by GLYCEROL-3-PHOSPHATE ACYLTRANSFERASES (GPATs) (Beisson et al., 2012). Additional cutin precursors are formed by enzymes of the BAHD family of acyltransferases, such as DEFECTIVE IN CUTICULAR RIDGES (DCR), which is essential for the incorporation of in-chain hydroxylated C16 fatty acids into cutin (Lashbrooke et al., 2016; Panikashvili et al., 2009). After export of cutin precursors to the apoplast, the formation of the cuticular polyester involves enzymes from the α/β hydrolase family, such as BODYGUARD (BDG), as well as cutin synthases from the GDSL-lipase family (Jakobson et al., 2016; Kurdyukov et al., 2006; Yeats et al., 2014).

Roots are very different from aerial organs as they generally grow in the soil and are specialized for the acquisition of water and nutrients, incompatible with the presence of a strong diffusion barrier at their entire surface. Indeed, in the primary growth stage, no visible lipid depositions are located at the surface of the root epidermis. Only deeper inside the root, the endodermis forms cell wall modifications with barrier functions, such as lignified Casparian strips as well as suberin lamellae (Doblas et al., 2017; Geldner, 2013). In addition to the primary root that originates from the embryo, lateral roots are initiated in the vascular cylinder of the primary root through divisions of the pericycle, leading to a branched root system (Van Norman et al., 2013). The emerging lateral root has to grow through the outer cell layers of the primary root, i.e., endodermis, cortex, and epidermis before breaking out, which is described as an invasive growth process (Marsollier and Ingram, 2018; Stoeckle et al., 2018). This lateral root outgrowth is accompanied by various cell and cell wall modifications that lead not only to changes in the anatomy of the overlaying endodermal cell and the breakdown of the Casparian strip, but also to separation of the outer cell layers at the respective positions. These processes are tightly regulated by the plant hormone auxin (Vermeer et al., 2014; Vilches-Barro and Maizel, 2015). After emergence, the lateral root matures establishing all typical cell types of the primary root.

The root cap at the tip of the root is an organ that protects the root meristem, promotes the growth of the root through the soil, and perceives and transmits environmental stimuli, including gravity and nutrient availability (Barlow, 2002; Kumpf and Nowack, 2015). Consisting of central columella cells and adjacent lateral root cap cells, the root cap has a determined size tightly balancing the continuous formation of new cells with elimination of old outer cells (Barlow, 2002). In *Arabidopsis*, the columella cells are sloughed off alive of the tip of the root. Lateral root cap cells are eliminated by programmed cell death, which starts at older cells next to the transition zone and progresses toward the columella cells. Dead and dying lateral root cap cells are detached together with the columella cells, such that the entire outermost root cap cell layer is eliminated in a coordinated manner (Fendrych et al., 2014; Kumpf and Nowack, 2015). Mature root cap cells form mucilage, rich in cell wall polysaccharides, such as pectins, thought to have a lubricant effect for the growth of the root in the soil (Durand et al., 2009).

A root cap is already formed early during the embryo development (Barlow, 2002). Although it is assumed that the root cap protects the root meristem in mature plants, little is known about the molecular mechanisms of root cap biology before the onset of the cell maturation and replacement cycles. Here, we show by histological, chemical, and genetic approaches that the first cell layer of the root cap of the primary root is covered by a hitherto unrecognized root cap cuticle (RCC). Structural modifications of the RCC at the primary root affect the diffusion barrier properties and lead to reduced rates of seedling establishment under osmotic stress and high salt conditions. Increased death of meristematic cells under high salt conditions indicates that the RCC protects the root meristem under stress conditions supporting thus seedling survival. RCC modifications at emerging lateral roots interfere with the process of lateral emergence as evidenced by a slower development of lateral roots and deformations of lateral root primordia reminiscent of organ adhesions. Our findings reveal a role for root caps in their early developmental stage and demonstrate that the RCC has equivalent physiological roles as the cuticle of the shoot.

RESULTS

A Cuticle Covers the Root Cap of the Primary Root

During the analysis of roots of 2-day-old *Arabidopsis thaliana* wild-type (WT) seedlings by transmission electron microscopy (TEM), we noticed that the surface of the cell wall of root cap cells was covered by an electron-opaque layer of 20 nm (18.5 ± 4.5 nm), resembling in thickness and ultrastructure the *Arabidopsis* leaf cuticle (Nawrath et al., 2013) (Figures 1A and 1B). This structure was not present at the root epidermis (Figures 1A and S1A).

The cuticle-like structure of the root cap was well defined from day 1 to 3 of seedling development, but less distinct at day 5, shortly before this first root cap layer is shed and replaced by the underlying, younger root cap layer (Figures 1A and S1B). The RCC was, however, already present at the radicle of the embryo (Figure S1C). Thus, the presence of this cell wall structure is tightly associated with the first root cap cell layer, which is formed during embryogenesis and shed from the seedling root ~5 days after germination (Dubreuil et al., 2018). The cuticle-like surface structure was also noticed in root caps of 2-day-old seedlings of *Brassica napus* and *Solanum lycopersicum* (Figure S1D), suggesting conservation of this root cap structure in higher plants.

In order to strengthen the hypothesis that this newly identified cell wall structure may be a layer containing aliphatic polyesters, fluorol yellow (FY), a dye staining aliphatic polyesters was used (Brundrett et al., 1991; Lux et al., 2005). FY stained the outer cell walls of root cap cells of 1- to 3-day-old WT seedlings (Figures 1B and S1B) but only rarely root caps of 5-day-old roots, confirming that only the first root cap layer generates a RCC (Figure S1B).

To discover the function of this transient RCC, the *CUTICLE DESTRUCTING FACTOR 1* (*CDEF1*) gene encoding an esterase of *Arabidopsis* able to degrade cutin and suberin (Barberon et al., 2016; Naseer et al., 2012; Takahashi et al., 2010) was expressed under the control of the promoter *pLOVE1* (*LOVE GLOVE1*), which is specifically active in the outermost layer of the root

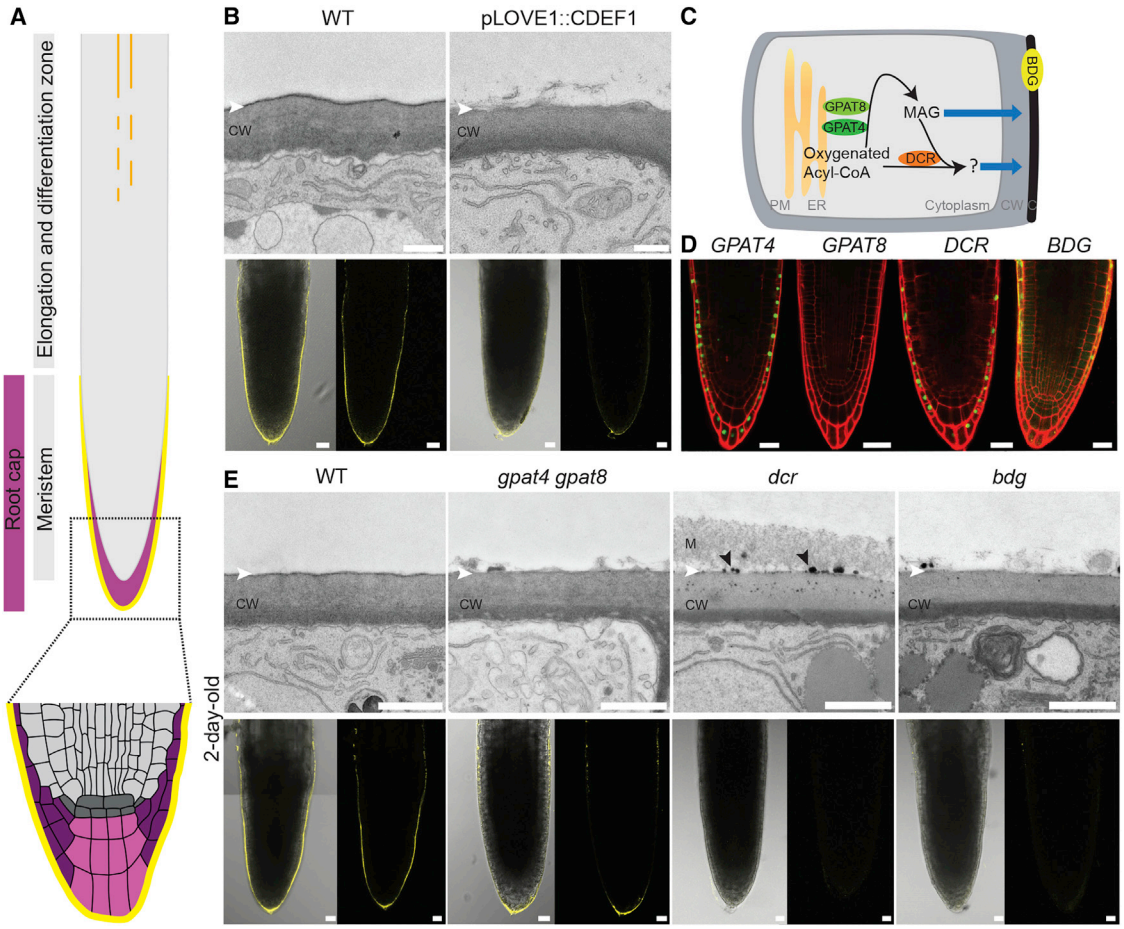

Figure 1. Evidence for a RCC at the Primary Root

(A) Schematic diagram highlighting polyester depositions in the roots of a 3-day-old *Arabidopsis* seedling. Orange, endodermal suberin; yellow, cuticle; pink, root cap cells. Enlargement: light gray, meristematic cells; dark gray, stem cells; light purple, columella cells; dark purple, lateral root cap cells; yellow, cuticle.

(B and E) TEM showing cell wall and cuticle of the outermost lateral root cap cells (top) and median views of the FY staining at the root cap of 2-day-old (B) WT and pLOVE1::CDEF1 plants and (E) WT and mutant plants affected in RCC biosynthesis (bottom; on the left, overlay bright field and fluorescence; on the right, fluorescence only). Scale bars in TEM pictures, 500 nm; in fluorescence micrographs, 20 μm. CW, cell wall; M, mucilage; white arrowhead, expected position of the cuticle; black arrowhead, methanol-soluble material. See also Figures S1 and S2.

(C) Simplified schematic diagram of the cutin biosynthetic pathway. Oxygenated acyl-CoA esters are generated at the endoplasmatic reticulum. They are metabolized by GPATs to monoacylglycerol and may be modified by DCR to precursors of unknown structure before being exported across the plasma membrane and the cell wall where cutin is formed in the cuticle, e.g., by the action of BDG. C, cuticle; CW, cell wall; ER, endoplasmatic reticulum; MAG, monoacylglycerol; PM, plasma membrane; blue arrow, export of precursors.

(D) Gene expression in transgenic plants expressing pGPAT::NLS-GFP-GUS, pDCR::NLS-GFP-GUS and pBDG::GFP at the root cap of a 2-day-old seedling. Scale bars, 20 μm.

cap. The root caps of 2-day-old plants expressing *pLOVE1::CDEF1* did not stain with FY and did not exhibit the electron-opaque cuticle-like layer in TEM (Figure 1B). Similarly, exogenously applied recombinant cutinase also removed the cuticle from the root cap (Figure S1E). Based on these findings, we classified the structural polyester of this newly discovered cell wall structure as a cutin.

Cutin Biosynthesis Genes Are Required for RCC Formation

We hypothesized if the RCC is made of cutin, then known cutin biosynthesis genes may be involved in its formation (Figure 1C). In fact, several genes that are required for the biosynthesis of cutin in organs of the shoot (i.e., *GPAT4*, *DCR*, and *BDG*) are also expressed in the root cap (Figure 1D). The *Arabidopsis* T-DNA knockout mutants *gpat4*, *dcr*, and *bdg* were selected for studying a putative role in RCC formation (Kurdyukov et al., 2006; Li et al., 2007; Panikashvili et al., 2009). Despite the absence of detectable *GPAT8* expression at the root cap (Figure 1C), *gpat8* and the *gpat4 gpat8* double mutants were also included in the study because *GPAT4* and *GPAT8* act redundantly in leaf cutin formation (Li et al., 2007). Impressively, no FY staining was visible at the RCC of *dcr* and *bdg* showing that *DCR* and *BDG* are required for RCC formation (Figure 1E). Similarly, the RCC of the *gpat4 gpat8* double mutant did not stain with FY (Figure 1E), while the RCC of the *gpat4* and *gpat8* single

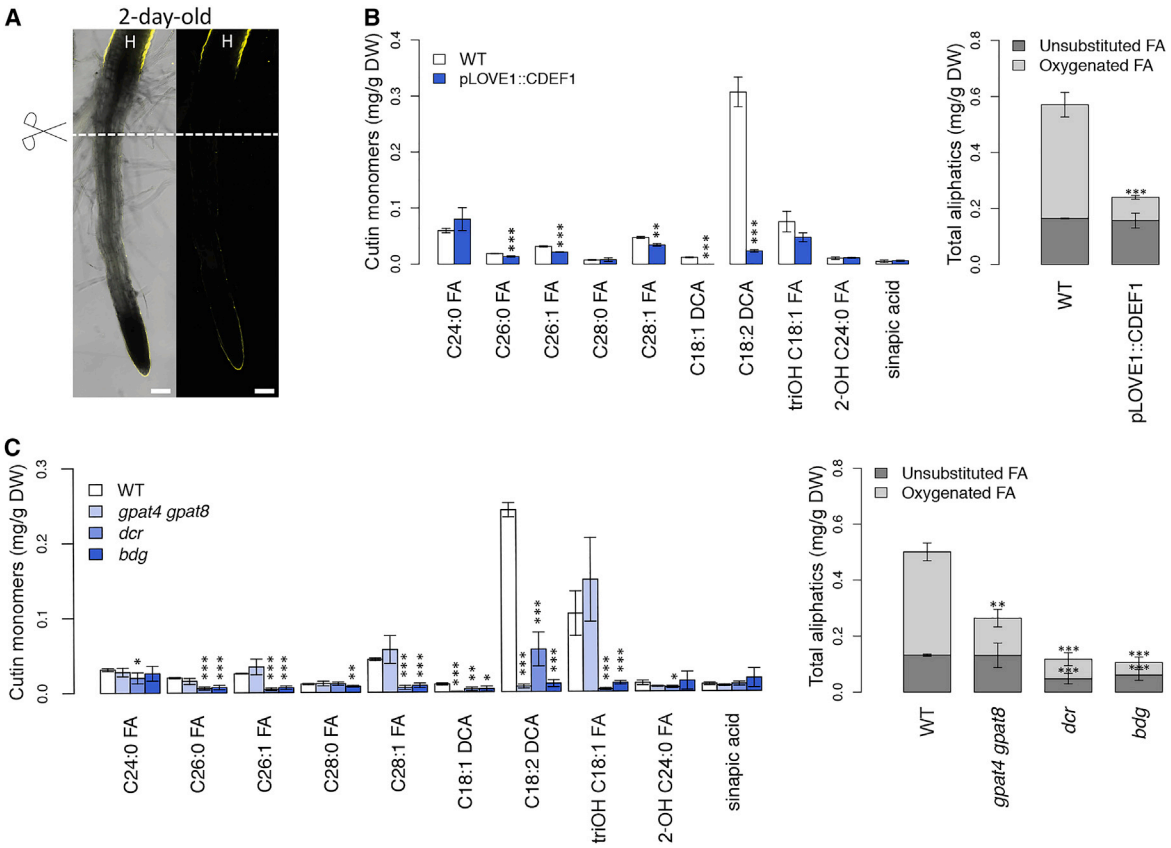

Figure 2. Composition of Cutin of the RCC at the Primary Root

(A) FY staining of the root of a 2-day-old seedling. H, hypocotyl; dashed line, point of sample excision for analysis. Scale bars, 100 μm.

(B and C) Quantification of aliphatic and aromatic ester-bond cutin monomers isolated from 2-day-old roots of (B) pLOVE1::CDEF1 plants and (C) RCC mutants, with their respective WT control. Left graph shows the principal cutin monomers and right graph shows the total of evaluated aliphatic compounds on the left grouped by substance classes. Values represent the means ± SD, n = 3–4. Asterisks denote significant differences to wild-type (WT) as determined by Student's t test: ***p < 0.001; **p < 0.01; *p < 0.05. FA, fatty acid; DCA, dicarboxylic acid; triOH C18:1 FA, 9,10,18-triOH C18:1 FA; DW, dry weight.

mutants stained as in WT (Figure S2A) demonstrating the redundant function of *GPAT4* and *GPAT8* in RCC formation.

TEM revealed that the RCC of *gpat4 gpat8* and *bdg* was less defined and had an eroded appearance (Figure 1E). In *dcr*, however, the continuous layer of cuticle was entirely absent and a broad layer of loose fibrous material, interpretated as mucilage, was present instead (Figure 1E). In addition, electron-dense globular structures were present within the outer half of the cell wall and at the cell wall-mucilage interface in the *dcr* mutant (Figure 1E). This material most likely consisted of unstructured and not completely polymerized cuticular lipids, because it was not visible when the sample was treated with methanol (Figure S2B). That the loosely attached fibrous material visible in TEM of the *dcr* mutant was indeed mucilage could be shown by immunolabeling with the xylogalacturonan-specific LM8 antibody that had been used previously to detect mucilage at *Arabidopsis* root cap cells (Durand et al., 2009) (Figure S2C). Our finding that genes necessary for cutin formation in leaves of *Arabidopsis* were also required for RCC formation further supports its structural analogy with the leaf cuticle.

Moreover, the receptor kinases GASSHO1/SCHENGEN3 (GSO1) and GASSHO2 (GSO2), acting redundantly in cuticle formation of the shoot (Tsuwamoto et al., 2008), act also together in RCC formation, as identified by FY staining (Figures S2D and S2E). TEM revealed, however, that the *gso1 gso2* double mutant has in addition to the disrupted cuticle strong modifications of the cell wall of the outer root cap cell layer (Figure S2E). Modifications of the RCC were also visible in the *smb* mutant defective in the root cap maturation process in TEM as well as by FY staining (Figure S2E).

In summary, RCC formation displays many parallels to shoot cuticle formation, in particular in cotyledons and leaves, but it is also integrated in the regulatory circuits of root cap maturation.

The Polyester of the RCC Represents an Atypical Cutin

In order to characterize the polyesters present in the RCC in more detail, the composition of the esterified lipids and aromatic acids bound to the cell wall were analyzed from root tips of 2-day-old *Arabidopsis* seedlings of different genotypes. We confirmed that at this age the endodermis was not yet suberized (Figure 2A), thus the entire lower root section could be used for the analysis. The most abundant oxygenated monomers of the cutin in the RCC were α,ω-octadecadiendioic acid (C18:2 DCA) and 9,10,18-trihydroxy octadecenoic acid (9,10,18-triOH

C18:1 FA) (Figures 2B and 2C), which are not present in endodermal suberin (Barberon et al., 2016). Despite these monomers indicating a C18 class cutin, very-long chain fatty acids of 26 and 28 carbons in length and their monounsaturated homologs were also present in considerable amounts, which is unusual for cutin (Figures 2B and 2C). Similarly unusual was that *p*-coumaric and ferulic acid, often present in cutin, could not be detected. Instead, sinapic acid was present as the only aromatic ester-bound compound. In summary, despite a high amount of oxygenated C18 fatty acids classically found in cutin, several atypical components were identified in the cell wall-bound ester fraction of the RCC.

In transgenic pLOVE1::CDEF1 plants expressing a cutinase specifically in root cap cells, predominant oxygenated fatty acids were reduced by 80%, while unsubstituted fatty acids as well as sinapic acid were not substantially altered (Figure 2B). In the *gpat4 gpat8* double mutant, the C18:2 DCA was reduced by more than 95% (Figure 2C). The *dcr* and *bdg* mutants showed both a strong reduction in oxygenated fatty acids and a less pronounced reduction of unsubstituted FAs (Figure 2C).

Taken together, the cutin in the RCC of the primary root has an atypical fatty acid composition requiring *GPAT4* and *GPAT8* as well as *DCR* and *BDG* for its synthesis, all of them also required for cutin formation in organs of the shoot.

The Emerging Lateral Root Is Also Covered by a Cuticle

Whether a cuticle is also present at the lateral root was investigated by TEM in 8-day-old WT *Arabidopsis* plants. An electron-opaque cuticle covered the cell wall of the outer most cell layer of the root cap of the lateral root before emergence and after emergence from the primary root (Figures 3A and 3B) that was thicker (36 ± 2.5 nm) than in primary roots. The RCC of the lateral roots stained in WT with FY, similar as in primary roots (Figure 3D). When the lateral root was fully differentiated, the FY staining was specific to the area of the root cap (Figure S3A).

The cutin biosynthesis genes *GPAT4* and *GPAT8* were also expressed at the outermost root cap cell layer in the developing lateral root (Figure 3C). Furthermore, gene expression of *BDG* and *DCR* had equally been reported at the lateral root tip (Jakobson et al., 2016; Panikashvili et al., 2009). Recently emerged lateral roots of *dcr*, *bdg*, and the *gpat4 gpat8* double mutant were characterized by TEM and subjected to the FY staining procedure. In contrast to a strong electron-opaque RCC in WT, the RCC of recently emerged lateral roots in *bdg* and the *gpat4 gpat8* was eroded and did not stain with FY (Figure 3D). *gpat4* and *gpat8* single mutants stained normally (Figure S3B). By contrast, the RCC of *dcr* mutants displayed alternating areas of electron-opaque cuticle and occasional disruptions, but still stained with FY (Figure 3D).

In summary, a cuticle covers root caps of both lateral and primary roots but differences in dimension, ultrastructure, and FY affinity in mutant genotypes indicate a different molecular structure and composition between the two RCCs.

Diffusion Barrier Properties Are Impaired in RCC Mutants

A hallmark of the role of the cuticle of aerial organs is to build a diffusion barrier (Schreiber, 2010). Barrier properties of the RCCs were assessed by dye diffusion assays across the cuticle using toluidine blue and fluorescein diacetate (Barberon et al., 2016; Li et al., 2007; Tanaka et al., 2004). Toluidine blue binds directly to anionic compounds that are present in the cell and in the apoplast (including pectic polysaccharides), while fluorescein diacetate is a cellular tracer that fluoresces only after uptake and cleavage in a living cell. Fluorescein diacetate allows live staining of single roots to highlight dynamic differences in staining between genotypes, while toluidine blue allows the simultaneous assessment of many roots (stained versus not stained).

Staining of the meristem of the primary root with fluorescein diacetate was too fast to allow the characterization of the RCC of the primary root by confocal microscopy (faster than 10 s). The permeability of the RCC of the primary root was thus assessed with toluidine blue in 2-day-old seedlings. In *Arabidopsis* WT plants, the number of roots having a stained meristem increased steadily between 20 s and 135 s, the time when the meristems of all the investigated roots were stained (Figure 4A). In contrast, a comparable staining of all root meristems was observed in pLOVE1::CDEF1 plants and the RCC mutants *bdg* and *dcr* already after 10 s and in the *gpat4 gpat8* double mutant after 20 s demonstrating diminished barrier properties of the RCC of the primary root in these genotypes (Figure 4A).

The barrier properties of the RCC of recently emerged lateral roots could be assessed by fluorescein diacetate. The tip of these lateral roots of WT did not show any fluorescence after a 4-min long incubation in fluorescein diacetate. In contrast, all the mutants that had modifications in the ultrastructure of the RCC at recently emerged lateral roots (i.e., *gpat4 gpat8*, *bdg*, and *dcr*) showed a clear fluorescence signal after a 4-min long incubation period demonstrating their diminished diffusion barrier properties. The strength of fluorescence depended on the genotype being the weakest in *gpat4 gpat8* and the strongest in *bdg* (Figure 4D).

In summary, both the RCC of the primary root as well as of the recently emerged lateral root provide barrier functions limiting the diffusion of molecules.

The RCC of the Primary Root Protects the Seedling against Harmful Compounds

Whether the diffusion barrier properties of the RCC of the primary root may be able to contribute to seedling establishment under abiotic stress conditions was tested in transgenic pLOVE1::CDEF1 lines. CDEF1 expression was restricted to the outermost cell layer of the radicle and young root, thus generating specifically a defective RCC. Mutants in cutin biosynthesis are affected in the deposition of several polyesters present in the seeds and are thus less suitable for these analyses (De Giorgi et al., 2015; Molina et al., 2008; Panikashvili et al., 2009). The development of transgenic pLOVE1::CDEF1 plants barely differed to WT under standard growth conditions. They were, however, much more strongly affected than WT by high salt concentrations (i.e., 100 mM NaCl, 75 mM K_2SO_4, and 100 mM KCl) or the osmotically active compound mannitol (250 mM) (Figure 4B) indicating that the RCC may protect establishing seedlings of harmful compounds.

Whether the RCC protects the meristematic cells of harmful components was investigated in the presence of NaCl because

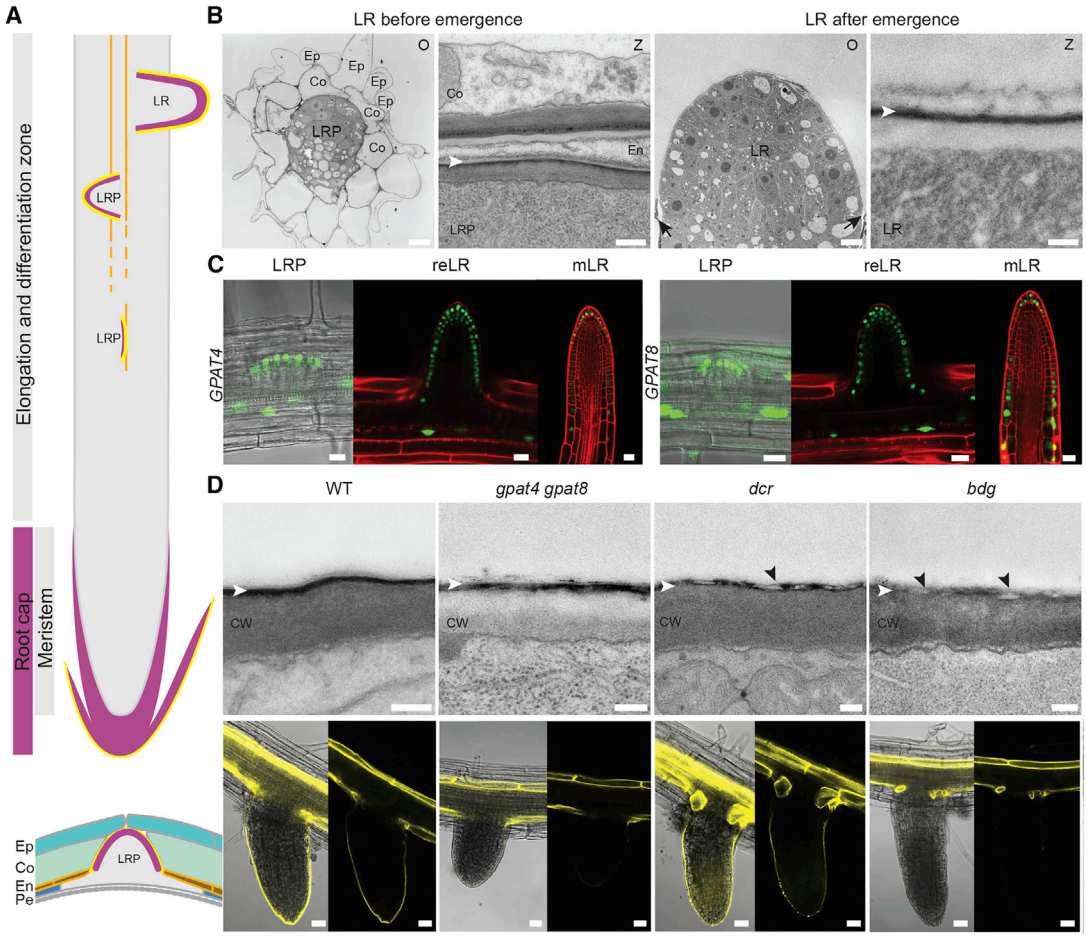

Figure 3. Evidence for a RCC at the Young Lateral Root

(A) Schematic diagram highlighting polyester depositions in a 5-day-old *Arabidopsis* seedling losing the first root cap cell layer. Orange, patchy and continuous suberin deposition; yellow, cuticle; pink, root cap cells. LRP, lateral root primordium; LR, lateral root; Co, cortical cell; En, endodermal cells; Ep, epidermal cell; Pe, pericycle.

(B) TEM showing the lateral root of WT before and after emergence. An overview (O) and an enlarged view (Z) of cell wall and cuticle at the root cap is given. The overview showing the lateral root before emergence was stitched together from multiple TEM pictures. Scale bars, 7 μm in O and 250 nm in Z. For details, see legend of (A); black arrow, cell wall of epidermal cells of the primary root; white arrowhead, expected position of the cuticle.

(C) Gene expression in transgenic plants expressing pGPAT::NLS-GFP-GUS at the lateral root of a 8-day-old seedling. LRP, lateral root promordium; reLR, recently emerged lateral root; mLR, maturelateral root. Scale bars, 20 μm.

(D) TEM pictures showing cell wall and cuticle (top) and median views of the FY staining of the developing lateral root of WT and mutant plants affected in RCC formation after emergence (bottom; on the left, overlay bright field and fluorescence; on the right, fluorescence only). FY stained the suberin of the endodermis and the RCC, when present. Scale bars, 200 nm in TEM pictures; 20 μm in pictures showing FY staining. CW, cell wall; white arrowhead, expected position of the cuticle; black arrowhead, eroded cuticle.

See also Figures S3A and S3B.

the excess of Na^+ ions is known to be toxic for cells and lead to cell death in *Arabidopsis* root tips (Olvera-Carrillo et al., 2015; Zhu, 2016). Propidium iodide, which only enters cells having a compromised plasma membrane integrity was used to identify the presence of dead cells (Truernit and Haseloff, 2008). In the presence of 140 mM NaCl, we found significantly more cell death in the root meristem of 2-day-old pLOVE1::CDEF1 seedlings than in WT (Figure 4C).

In summary, the RCC of the primary root having diffusion barrier functions protect the meristematic cells from toxic compounds during the vulnerable growth stage of seedling establishment.

RCC Defects at Lateral Root Primordia Lead to Delayed Outgrowth of Lateral Roots

Because genes involved in RCC formation of lateral roots are already expressed before lateral root emergence, and the cuticle is well-defined while the lateral root invades the tissues of the primary root (Figure 3B), we investigated whether the RCC of the lateral root primordium may play a role in the process of lateral root emergence. When lateral root initiation was synchronized in vertically growing roots by turning the agar plates by 90° (Voß et al., 2015), the majority of the lateral roots of WT had emerged after 42 h, while the lateral primordia of *gpat4 gpat8*, *dcr*, and *bdg* were still in the outer tissue layers of the primary root (Figure 4E).

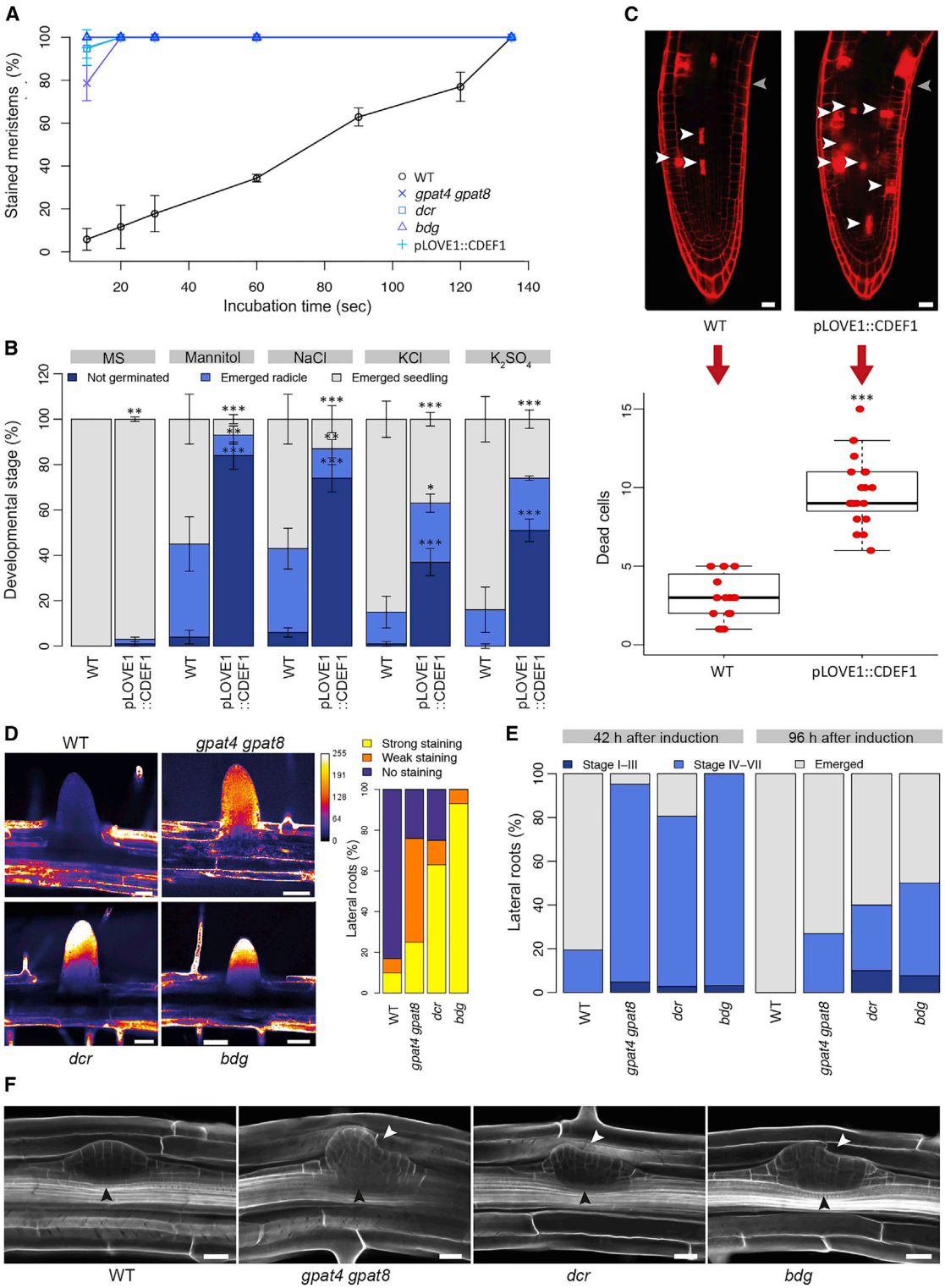

Figure 4. Diffusion Barrier Properties and Biological Roles of RCCs

(A) Penetration of toluidine blue into the meristem of 2-day-old seedlings of different genotypes. Values represent the mean ± SD of the number of stained meristems in a seedling population at indicated time points.

(B) Role of the RCC of primary roots in seed germination and seedling establishment illustrated by studying the impact of mannitol (250 mM), NaCl (100 mM), KCl (100 mM), and K_2SO_4 (75 mM) in the medium during early root development stages on WT and pLOVE1::CDEF1 plants. Values represent the mean ± SD of the

(legend continued on next page)

Even after 96 h, a certain number of lateral root primordia of the RCC mutants had not yet broken through the epidermis, even when the outgrowth process had further advanced, demonstrating a severe retardation of the lateral root emergence process in mutants having RCC defects at lateral root primordia (Figure 4E).

Cuticles of the shoot play an important role during the development of organs by preventing surface interactions when plant organs are in tight contact because cuticle impairments may lead to organ adhesions and fusions (Ingram and Nawrath, 2017). Therefore, we investigated the shape of lateral root primordia during the lateral root emergence process. Deformations of lateral root primordia occurred during the passage through the cortex layer in all three genotypes having RCC modifications at the lateral root primordia (Figures 4F and S3). Such deformations could never be observed at lateral root primordia of WT (Figures 4F and S3). Deformed lateral root primordia could be observed in 5%–11% of the total investigated roots at early (42 h and 48 h) observation times and were not more, but rather less frequent at later observation times (96 h) (2%–7%) indicating that they were a transient phenomenon during the emergence process. The deformations of the lateral root primordia in RCC mutants suggest that the RCC facilitates invasive growth of the lateral root primordia by reducing cell surface interactions causing organ adhesions.

DISCUSSION

The RCC Defines an Early Developmental Stage of Root Caps

Up to now, the root cap has been understood as a structure secreting mucilage and releasing their older cells as single border cells or cell clusters (Barlow, 2002). While this is true for root caps with rapid cell turn-over, our ultrastructure analysis of the cell wall of root caps before the onset of the root cap turnover cycle has revealed an as yet undocumented structure, the root cap cuticle (RCC). Because the RCC is only present on the very first root cap cell layer of primary and lateral roots, it defines a specific developmental and physiological state of root caps.

The Formation of the RCC Is Integrated in Root Cap Cell Differentiation

The receptor kinases GSO1 and GSO2 are required for establishing epidermis-specific functions of cotyledons during embryo development and during seedling establishment in *Arabidopsis* (Tsuwamoto et al., 2008; Xing et al., 2013). Both GSO1 and GSO2 are also essential for the proliferation and differentiation of root cell types in young seedlings, including columella and lateral root cap cells (Racolta et al., 2014). The *gso1 gso2* double mutant, but not both single mutants, has an interrupted RCC at the primary root indicating that *GSO1* and *GSO2* act redundantly in RCC formation. An adherence of the endosperm to the embryo was documented in embryos of the *gso1 gso2* double mutant (Moussu et al., 2017), indicating that these genes are important for generating the appropriate surface structure of organs before and after seedling germination. Interestingly, *GSO2* exhibits an intriguing change in expression from strong root cap expression at 3 days after germination (i.e., when the root cap has a cuticle) to none at 6 days after germination (i.e., when root cap cells have no RCC anymore) (Racolta et al., 2014). This expression pattern underscores that the root cap of young establishing seedlings has different characteristics than the one of older plants.

An additional argument that the formation of the RCC is tightly regulated during the development and differentiation of root cap cells is that the *smb* mutant having a delayed maturation of root cap cells has also a defective RCC (Bennett et al., 2010).

The *Arabidopsis* RCC Consists of a Particular Cutin

The ultrastructure of the RCC was visualized as an electron-opaque layer that resembled the leaf cuticle of *Arabidopsis* WT plants (Nawrath et al., 2013). Indeed, the cutin of the RCC was rich in two components: (1) C18:2 DCA that is the predominate cutin monomer in *Arabidopsis* leaves, but is rather atypical for cutin within the plant kingdom (Bonaventure et al., 2004; Franke et al., 2005), and (2) 9,10,18-triOH C18:1 FA that is a prominent cutin monomer in many species (Beisson et al., 2012; Kolattukudy, 2001a), but is typically absent from any *Arabidopsis* shoot cuticle. As in other organs of *Arabidopsis*, *GPAT4* and *GPAT8* were required for the incorporation of C18:2 DCA in the polyester of the RCC (Li et al., 2007). The incorporation of 9,10,18-triOH C18:1 FA depended strongly on DCR emphasizing the important role of this acyltransferase for the incorporation of mid-chain hydroxylated fatty acids into cutin (Lashbrooke et al., 2016; Panikashvili et al., 2009). BDG plays an important role for the incorporation of C18:2 DCA into cutin of *Arabidopsis* leaves and flowers but leading only to moderate (40%–50%) reductions in the polyester amount of these organs in *bdg* (Jakobson et al., 2016). Here, we

number of seedlings of each genotype having the indicated stage when grown in the presence of the respective compound. Significant differences to WT were determined by Student's t test: ***$p < 0.001$; **$p < 0.01$; *$p < 0.05$.

(C) Salt-induced cell death in the meristem of 2-day-old root of WT and pLOVE1::CDEF1 plants. Dead cells present after a 10-min-long incubation in 140 mM NaCl are visualized by propidium iodide staining. Top: Pictures show the median section of the root tip. White arrowhead, dead cell; gray arrowhead, superior limit of the meristematic zone. Scale bars, 20 μm. Bottom: The number of dead cells present in the entire meristematic zone of each root (as assessed via a z stack) are presented as boxplot. Individual data points are shown as dots. Asterisks denote significant differences to WT as determined by Student's t test: ***$p < 0.001$.

(D) Penetration of the fluorescent cellular tracer fluorescein diacetate into root cap cells and meristematic cells of shortly emerged lateral roots of different genotypes after 4 min of incubation. Relative intensity of the fluorescence is depicted by the color code. Scale bars, 50 μm. Quantitative evaluation is given in the graph to the right showing the number of shortly emerged lateral roots having the indicated staining intensity.

(E and F) Role of the RCC at the lateral root primordium during lateral root emergence. (E) Stages of lateral root primordia 42 h and 96 h after induction were evaluated in WT and in different mutant genotypes having a modified RCC at the lateral root primordium. Stages were determined as described in Casimiro et al. (2003): stage I–III, before breakage into the cortex; stage IV–VII, within the outer layers of the primary root; emerged. (F) Shape of lateral root primordia in WT and different genotypes having a modified RCC at the emerging lateral root. Regular shape of a lateral root primordium of WT. Deformed lateral root primordia of genotypes having RCC modifications at the lateral root. Black arrowhead, lateral root primordium; white arrowhead, primordium deformation. Scale bars, 20 μm. See also Figure S3C.

showed that BDG is also required for the incorporation for 9,10,18-triOH C18:1 FA into cutin resulting in a particular strong reduction (80%) in the total polyester content of the RCC of primary roots in *bdg*. Overall, the incorporation of oxygenated monomers into cutin of the RCC occurs very well in accordance with our current understanding of cutin synthesis in *Arabidopsis* (Fich et al., 2016; Nawrath et al., 2013). In the future, the RCC might be a useful tool for studying the incorporation and the functional relevance of its atypical polyester monomers (i.e., C26 and C28 acids as well as sinapic acid).

The RCC had a different ultrastructure during the course of development of root cap cells analogous to maturing cuticles in aerial tissues. In aerial tissues, changes in the cuticle ultrastructure are associated with changes in cutin composition, structure, and properties (Fabre et al., 2016; Jeffree, 2006; Nawrath et al., 2013), which still would need to be investigated in more detail for the RCC.

The RCCs of Primary and Emerging Lateral Roots Form a Diffusion Barrier

One of the principal and best-studied features of cuticles of the shoot is that they form a diffusion barrier separating the respective plant organ from the surrounding environment (Riederer, 2006). The barrier properties of the cuticle of different species and organs of the same species vary widely (Schreiber and Schönherr, 2009). Nevertheless, the cuticles have protective functions in their respective cellular context. The incubation time necessary to stain the meristem below the RCC of the primary root was shorter than for tissues below shoot cuticles grown under similar conditions (Moussu et al., 2017; Tanaka et al., 2004). The cellular processes in root cap cells as well as the environmental conditions below-ground differ from shoots where cuticles are in an aerial environment. This might explain why the RCCs evolved different properties. It may also be an argument for aliphatic wax molecules, typically associated with leaf cuticles, being the important determinant for the transport barrier properties of cuticles, more than the amount and composition of the cutin polyester itself (Kosma et al., 2009; Schreiber, 2010; Zeisler-Diehl et al., 2018). Whether the cutin in the RCC is associated with some type of waxes remains to be elucidated.

The RCC of the Primary Root Protects the Root Meristem

The cuticle of the shoot with its function as diffusion barrier influences the uptake and loss of a wide variety of molecules, including water, nutrients, volatiles, and toxic compounds (Riederer, 2006; Schreiber and Schönherr, 2009; Valeska Zeisler-Diehl et al., 2017). The hypersensitivity of plants having a permeable RCC to hyperosmotic conditions and salt stress indicate that the RCC has similar broad functions as diffusion barrier at the root cap during seedling establishment. Because diffusion barriers function in both directions (i.e., in uptake and loss of solutes), the RCC may prevent an even faster water loss under osmotic stress conditions that would cause an irreversible cell damage. During salt stress, not only water is lost by the osmotic differential, but also ions will diffuse into the plant reaching toxic concentrations faster than when a RCC is present. Higher death rates of meristematic cells in the presence of toxic concentrations of NaCl could be observed in pLOVE1::CDEF1 plants supporting this hypothesis. Even though a transient structure, the results point to crucial role of the RCC of primary roots in protecting the meristem in the stage when it is very small and highly susceptible to stress conditions and thus gives the seedling some time to adapt and to put other protective mechanisms in place (Zhu, 2016).

Cuticles of the shoot are also implicated in the interaction of plants with its microbial environment. Susceptibility or resistance of the plant are the outcome of complex processes that are not predictable solely based on structure, amount, and composition of the cuticle (Ziv et al., 2018). Sensitivity of seedling establishment toward biotic stresses has recently been shown by inhibition of germination in the presence of bacterial pathogens (Chahtane et al., 2018). Whether the protective functions of the RCC will also extend to the interaction with the biotic environment will be a topic of future studies.

The RCC of the Lateral Root Promotes Lateral Root Emergence

Lateral root formation, one of the key steps for the adaptive remodeling of root system architecture, determines the efficiency of the root in nutrient acquisition. The mechanisms of lateral root emergence are therefore a focus of current plant research (Stoeckle et al., 2018; Van Norman et al., 2013; Vilches-Barro and Maizel, 2015). Lateral root emergence is an invasive growth process (Marsollier and Ingram, 2018) because the lateral root primordia, initiated at the pericycle deeply within the primary root, have to penetrate through the different overlying tissue layers to emerge (Figure 3A). During the entire emergence process the lateral root primordium is in very tight contact with the surrounding tissue layers. Therefore, the presence of a substance functioning as ''lubricant'' during lateral root emergence has been hypothesized (Marsollier and Ingram, 2018). Here, we showed that lateral roots having impairments in the RCC of the primordium are strongly slowed down during the emergence process and have deformations giving experimental evidence for a role of the RCC of the lateral root primordia in the prevention of surface interactions of different organs.

The cuticle of aerial organs has important functions in the prevention of organ adhesions during plant development that manifest themselves in organ deformations (e.g., during the rapid outgrowth of petals from the floral bud) (Ingram and Nawrath, 2017). Under certain circumstances, fusions between organs of the shoot may be seen in plants having a permeable shoot cuticle that are characterized by the formation of a single cell wall between the organs and tissue breakage when the fusion is disrupted (Nawrath et al., 2013). In the investigated RCC mutants, no signs have been observed that deformations at the lateral root primordium were solved by tissue breakage or remained permanent, but instead a decrease in the number of organ deformations over time, indicating that organ adhesions, not organ fusions, occurred.

Interestingly, the radicle of the *gso1 gso2* double mutant did not separate from the endosperm (Moussu et al., 2017) suggesting that a cuticular structure on the radicle might have similar functions in preventing organ adhesions during embryo development.

Conclusions

Plant cuticles of different aerial organs have been studied since the middle of the 19th century and have so far been exclusively associated with epidermal tissues of the shoot. Suberin lamellae, by contrast, have been seen in many other tissues of shoots and roots (Holloway, 1982b; Kolattukudy, 1980; Pollard et al., 2008). Therefore, it has been deduced that only shoot epidermal cells and protodermal cells of the embryo, as their precursor, can synthetize a cuticle, and not root tissues (Barlow, 2002). Our discovery of a cuticle at the root cap now challenges this dogma.

The RCC of young primary roots and emerging lateral roots play important roles in root physiology and development. During the critical first days after germination, the RCC serves as a diffusion barrier, protecting the vulnerable seedling meristem and giving thus the seedling some time to adapt to environmental challenges. In lateral root formation, the RCC serves as a specialized surface structure that prevents adhesions of newly forming organs, similar as the cuticle of aerial organs does. The discovery of the RCC adds a new element to our understanding of root anatomy, development, and physiology.

STAR★METHODS

Detailed methods are provided in the online version of this paper and include the following:

- KEY RESOURCES TABLE
- CONTACT FOR REAGENT AND RESOURCE SHARING
- EXPERIMENTAL MODEL AND SUBJECT DETAILS
  - Plant material
  - Growth conditions
- METHOD DETAILS
  - Generation of constructs
  - Cutin digestion, cuticle staining and permeability assays
  - Germination and root growth assays
  - Immunofluorescence labeling
  - Fluorescence Microscopy
  - Transmission electron microscopy
  - Chemical analyses
- QUANTIFICATION AND STATISTICAL ANALYSIS

SUPPLEMENTAL INFORMATION

Supplemental Information includes four figures and one table and can be found with this article online at https://doi.org/10.1016/j.cell.2019.01.005.

ACKNOWLEDGMENTS

We greatly appreciated helpful discussions and technical advice of Robertas Ursache, Tonni Anderson, Peter Marhavy, Evangelia Vogiatzaki, Steven Moussu, and Gwyneth Ingram. Particular thanks go to Niko Geldner and Marie Barberon for their discussions, sharing of unpublished information, and critical comments on the manuscript. Furthermore, we thank Willy Blanchard for his contribution to the artwork. The NASC stock center, Fred Beisson, Gwyneth Ingram, Liina Jakobson, and Niko Geldner are thanked for providing us with seed stocks and Mario Serrano for supplying us with cutinase. Furthermore, we thank Bruno Humbel and Arnaud Paradis for leading the Electron Microscopy Facility and the Imaging Facility of UNIL, respectively. This work was supported by the Swiss National Science Foundation (31003A_170127 to C.N.) and the ERC (starting grant PROCELLDEATH; Project Number 639234 to M.K.N.).

AUTHOR CONTRIBUTIONS

Conceptualization, A.B., C.N., and M.K.N.; Methodology, A.B. and D.d.B.; Investigation, A.B. and D.d.B., Validation, A.B., R.B.F., and C.N.; Resources, R.A.B. and M.K.N.; Writing–Initial Draft, C.N.; Writing–Review & Editing, A.B., M.K.N., and R.B.F., Visualization, A.B., Supervision and Funding Acquisition, C.N.

DECLARATION OF INTERESTS

The authors declare no competing interests.

Received: June 30, 2018
Revised: November 23, 2018
Accepted: January 2, 2019
Published: February 14, 2019

REFERENCES

Alberts, B., Johnson, A., Lewis, J., Morgan, D., Raff, M., Roberts, K., and Walter, P. (2015). Molecular Biology of the Cell, Sixth Edition (Garland Science, Taylor and Francis Group).

Ali, M.A., Shah, K.H., and Bohlmann, H. (2012). pMAA-Red: a new pPZP-derived vector for fast visual screening of transgenic Arabidopsis plants at the seed stage. BMC Biotechnol. *12*, 37.

Andersen, T.G., Barberon, M., and Geldner, N. (2015). Suberization - the second life of an endodermal cell. Curr. Opin. Plant Biol. *28*, 9–15.

Bakan, B., and Marion, D. (2017). Assembly of the cutin polyester: from cells to extracellular cell walls. Plants (Basel) *6*, E57.

Barberon, M., Vermeer, J.E.M., De Bellis, D., Wang, P., Naseer, S., Andersen, T.G., Humbel, B.M., Nawrath, C., Takano, J., Salt, D.E., and Geldner, N. (2016). Adaptation of root function by nutrient-induced plasticity of endodermal differentiation. Cell *164*, 447–459.

Barlow, P.W. (2002). The root cap: cell dynamics, cell differentiation and cap function. J. Plant Growth Regul. *21*, 261–286.

Beisson, F., Li-Beisson, Y., and Pollard, M. (2012). Solving the puzzles of cutin and suberin polymer biosynthesis. Curr. Opin. Plant Biol. *15*, 329–337.

Bennett, T., van den Toorn, A., Sanchez-Perez, G.F., Campilho, A., Willemsen, V., Snel, B., and Scheres, B. (2010). SOMBRERO, BEARSKIN1, and BEARSKIN2 regulate root cap maturation in Arabidopsis. Plant Cell *22*, 640–654.

Bonaventure, G., Beisson, F., Ohlrogge, J., and Pollard, M. (2004). Analysis of the aliphatic monomer composition of polyesters associated with Arabidopsis epidermis: occurrence of octadeca-cis-6, cis-9-diene-1,18-dioate as the major component. Plant J. *40*, 920–930.

Brundrett, M.C., Kendrick, B., and Peterson, C.A. (1991). Efficient lipid staining in plant material with sudan red 7B or fluorol [correction of fluoral] yellow 088 in polyethylene glycol-glycerol. Biotech. Histochem. *66*, 111–116.

Casimiro, I., Beeckman, T., Graham, N., Bhalerao, R., Zhang, H., Casero, P., Sandberg, G., and Bennett, M.J. (2003). Dissecting Arabidopsis lateral root development. Trends Plant Sci. *8*, 165–171.

Chahtane, H., Nogueira Füller, T., Allard, P.M., Marcourt, L., Ferreira Queiroz, E., Shanmugabalaji, V., Falquet, J., Wolfender, J.L., and Lopez-Molina, L. (2018). The plant pathogen *Pseudomonas aeruginosa* triggers a DELLA-dependent seed germination arrest in *Arabidopsis*. eLife *7*, e37082.

Clough, S.J., and Bent, A.F. (1998). Floral dip: a simplified method for Agrobacterium-mediated transformation of *Arabidopsis thaliana*. Plant J. *16*, 735–743.

De Giorgi, J., Piskurewicz, U., Loubery, S., Utz-Pugin, A., Bailly, C., Mène-Saffrané, L., and Lopez-Molina, L. (2015). An endosperm-associated cuticle is

required for Arabidopsis seed viability, dormancy and early control of germination. PLoS Genet. *11*, e1005708.

Doblas, V.G., Geldner, N., and Barberon, M. (2017). The endodermis, a tightly controlled barrier for nutrients. Curr. Opin. Plant Biol. *39*, 136–143.

Dominguez, E., Mercado, J.A., Quesada, M.A., and Heredia, A. (1999). Pollen sporopollenin: degradation and structural elucidation. Sex. Plant Reprod. *12*, 171–178.

Dubreuil, C., Jin, X., Grönlund, A., and Fischer, U. (2018). A local auxin gradient regulates root cap self-renewal and size homeostasis. Curr. Biol. *28*, 2581–2587.e3.

Durand, C., Vicré-Gibouin, M., Follet-Gueye, M.L., Duponchel, L., Moreau, M., Lerouge, P., and Driouich, A. (2009). The organization pattern of root border-like cells of Arabidopsis is dependent on cell wall homogalacturonan. Plant Physiol. *150*, 1411–1421.

Fabre, G., Garroum, I., Mazurek, S., Daraspe, J., Mucciolo, A., Sankar, M., Humbel, B.M., and Nawrath, C. (2016). The ABCG transporter PEC1/ABCG32 is required for the formation of the developing leaf cuticle in Arabidopsis. New Phytologist *209*, 192–201.

Fendrych, M., Van Hautegem, T., Van Durme, M., Olvera-Carrillo, Y., Huysmans, M., Karimi, M., Lippens, S., Guérin, C.J., Krebs, M., Schumacher, K., and Nowack, M.K. (2014). Programmed cell death controlled by ANAC033/SOMBRERO determines root cap organ size in Arabidopsis. Curr. Biol. *24*, 931–940.

Fich, E.A., Segerson, N.A., and Rose, J.K.C. (2016). The plant polyester cutin: biosynthesis, structure, and biological roles. Annu. Rev. Plant Biol. *67*, 207–233.

Franke, R., Briesen, I., Wojciechowski, T., Faust, A., Yephremov, A., Nawrath, C., and Schreiber, L. (2005). Apoplastic polyesters in Arabidopsis surface tissues–a typical suberin and a particular cutin. Phytochemistry *66*, 2643–2658.

Franke, R.B., Dombrink, I., and Schreiber, L. (2012). Suberin goes genomics: use of a short living plant to investigate a long lasting polymer. Front. Plant Sci. *3*, 4.

Geldner, N. (2013). The endodermis. Annu. Rev. Plant Biol. *64*, 531–558.

Holloway, P.J. (1982a). The chemical constitution of plant cutins. In The Plant Cuticle, D.F. Cutler, K.L. Alvin, and C.E. Price, eds. (Academic Press), pp. 45–86.

Holloway, P.J. (1982b). Structure and histochemistry of plant cuticular membranes: An overview. In The Plant Cuticle, D.F. Cutler, K.L. Alvin, and C.E. Price, eds. (Academic Press), pp. 1–32.

Ingram, G., and Nawrath, C. (2017). The roles of the cuticle in plant development: organ adhesions and beyond. J. Exp. Bot. *68*, 5307–5321.

Jakobson, L., Lindgren, L.O., Verdier, G., Laanemets, K., Brosché, M., Beisson, F., and Kollist, H. (2016). BODYGUARD is required for the biosynthesis of cutin in Arabidopsis. New Phytol. *211*, 614–626.

Jeffree, C.E. (2006). The fine structure of the plant cuticle. In Biology of the Plant Cuticle, M. Riederer and C. Müller, eds. (Blackwell Publishing), pp. 11–125.

Kolattukudy, P.E. (1980). Cutin, suberin and waxes. In The Biochemistry of Plants,, *vol. IV*, P.K. Stumpf, ed. (Academic Press), pp. 571–645.

Kolattukudy, P.E. (2001a). Cutin from plants. In Biopolymers, Y. Doi and A. Steinbüchel, eds. (Wiley-VCH), pp. 1–35.

Kolattukudy, P.E. (2001b). Suberin from plants. In Biopolymers, Y. Doi and A. Steinbüchel, eds. (Wiley-VCH), pp. 41–68.

Kosma, D.K., Bourdenx, B., Bernard, A., Parsons, E.P., Lü, S., Joubès, J., and Jenks, M.A. (2009). The impact of water deficiency on leaf cuticle lipids of Arabidopsis. Plant Physiol. *151*, 1918–1929.

Kumpf, R.P., and Nowack, M.K. (2015). The root cap: a short story of life and death. J. Exp. Bot. *66*, 5651–5662.

Kurdyukov, S., Faust, A., Nawrath, C., Bär, S., Voisin, D., Efremova, N., Franke, R., Schreiber, L., Saedler, H., Métraux, J.P., and Yephremov, A. (2006). The epidermis-specific extracellular BODYGUARD controls cuticle development and morphogenesis in Arabidopsis. Plant Cell *18*, 321–339.

Lashbrooke, J., Cohen, H., Levy-Samocha, D., Tzfadia, O., Panizel, I., Zeisler, V., Massalha, H., Stern, A., Trainotti, L., Schreiber, L., et al. (2016). MYB107 and MYB109 homologues regulate suberin deposition in angiosperms. Plant Cell *28*, 2097–2116.

Li, Y., Beisson, F., Koo, A.J.K., Molina, I., Pollard, M., and Ohlrogge, J. (2007). Identification of acyltransferases required for cutin biosynthesis and production of cutin with suberin-like monomers. Proc. Natl. Acad. Sci. USA *104*, 18339–18344.

Li-Beisson, Y., Shorrosh, B., Beisson, F., Andersson, M.X., Arondel, V., Bates, P.D., Baud, S., Bird, D., Debono, A., Durrett, T.P., et al. (2013). Acyl-lipid metabolism. Arabidopsis Book *11*, e0161.

Lux, A., Morita, S., Abe, J., and Ito, K. (2005). An improved method for clearing and staining free-hand sections and whole-mount samples. Ann. Bot. *96*, 989–996.

Malamy, J.E., and Benfey, P.N. (1997). Organization and cell differentiation in lateral roots of Arabidopsis thaliana. Development *124*, 33–44.

Marsollier, A.-C., and Ingram, G. (2018). Getting physical: invasive growth events during plant development. Curr. Opin. Plant Biol. *46*, 8–17.

Molina, I., Bonaventure, G., Ohlrogge, J., and Pollard, M. (2006). The lipid polyester composition of *Arabidopsis thaliana* and *Brassica napus* seeds. Phytochemistry *67*, 2597–2610.

Molina, I., Ohlrogge, J.B., and Pollard, M. (2008). Deposition and localization of lipid polyester in developing seeds of *Brassica napus* and *Arabidopsis thaliana*. Plant J. *53*, 437–449.

Moussu, S., Doll, N.M., Chamot, S., Brocard, L., Creff, A., Fourquin, C., Widiez, T., Nimchuk, Z.L., and Ingram, G. (2017). ZHOUPI and KERBEROS mediate embryo/endosperm separation by promoting the formation of an extracuticular sheath at the embryo surface. Plant Cell *29*, 1642–1656.

Naseer, S., Lee, Y., Lapierre, C., Franke, R., Nawrath, C., and Geldner, N. (2012). Casparian strip diffusion barrier in Arabidopsis is made of a lignin polymer without suberin. Proc. Natl. Acad. Sci. USA *109*, 10101–10106.

Nawrath, C., Schreiber, L., Franke, R.B., Geldner, N., Reina-Pinto, J.J., and Kunst, L. (2013). Apoplastic diffusion barriers in Arabidopsis. Arabidopsis Book *11*, e0167.

Olvera-Carrillo, Y., Van Bel, M., Van Hautegem, T., Fendrych, M., Huysmans, M., Simaskova, M., van Durme, M., Buscaill, P., Rivas, S., Coll, N.S., et al. (2015). A conserved core of programmed cell death indicator genes discriminates developmentally and environmentally induced programmed cell death in plants. Plant Physiol. *169*, 2684–2699.

Panikashvili, D., Shi, J.X., Schreiber, L., and Aharoni, A. (2009). The Arabidopsis *DCR* encoding a soluble BAHD acyltransferase is required for cutin polyester formation and seed hydration properties. Plant Physiol. *151*, 1773–1789.

Pfister, A., Barberon, M., Alassimone, J., Kalmbach, L., Lee, Y., Vermeer, J.E.M., Yamazaki, M., Li, G., Maurel, C., Takano, J., et al. (2014). A receptor-like kinase mutant with absent endodermal diffusion barrier displays selective nutrient homeostasis defects. eLife *3*, e03115.

Pollard, M., Beisson, F., Li, Y., and Ohlrogge, J.B. (2008). Building lipid barriers: biosynthesis of cutin and suberin. Trends Plant Sci. *13*, 236–246.

Racolta, A., Bryan, A.C., and Tax, F.E. (2014). The receptor-like kinases GSO1 and GSO2 together regulate root growth in Arabidopsis through control of cell division and cell fate specification. Dev. Dyn. *243*, 257–278.

Riederer, M. (2006). Introduction: biology of the plant cuticle. In Biology of the Plant Cuticle, M. Riederer and C. Müller, eds. (Blackwell Publishing), pp. 1–10.

RStudio Team (2015). RStudio: Integrated Development for R. RStudio, Inc., Boston, MA. https://www.rstudio.com.

Schindelin, J., Arganda-Carreras, I., Frise, E., Kaynig, V., Longair, M., Pietzsch, T., Preibisch, S., Rueden, C., Saalfeld, S., Schmid, B., et al. (2012). Fiji: an open-source platform for biological-image analysis. Nat. Methods *9*, 676–682.

Schreiber, L. (2010). Transport barriers made of cutin, suberin and associated waxes. Trends Plant Sci. *15*, 546–553.

Schreiber, L., and Schönherr, J. (2009). Water and Solute Permeability of Plant Cuticles (Springer Berlin Heidelberg).

Stoeckle, D., Thellmann, M., and Vermeer, J.E.M. (2018). Breakout-lateral root emergence in *Arabidopsis thaliana*. Curr. Opin. Plant Biol. *41*, 67–72.

Szczuka, E., and Szczuka, A. (2003). Cuticle fluorescence during embryogenesis of *Arabidopsis thaliana* (L.) Heynh. Acta Biol. Cracov. Ser. Bot. *45*, 63–67.

Takahashi, K., Shimada, T., Kondo, M., Tamai, A., Mori, M., Nishimura, M., and Hara-Nishimura, I. (2010). Ectopic expression of an esterase, which is a candidate for the unidentified plant cutinase, causes cuticular defects in *Arabidopsis thaliana*. Plant Cell Physiol. *51*, 123–131.

Tanaka, T., Tanaka, H., Machida, C., Watanabe, M., and Machida, Y. (2004). A new method for rapid visualization of defects in leaf cuticle reveals five intrinsic patterns of surface defects in Arabidopsis. Plant J. *37*, 139–146.

Truernit, E., and Haseloff, J. (2008). A simple way to identify non-viable cells within living plant tissue using confocal microscopy. Plant Methods *4*, 15.

Tsuwamoto, R., Fukuoka, H., and Takahata, Y. (2008). *GASSHO1* and *GASSHO2* encoding a putative leucine-rich repeat transmembrane-type receptor kinase are essential for the normal development of the epidermal surface in Arabidopsis embryos. Plant J. *54*, 30–42.

Ursache, R., Andersen, T.G., Marhavý, P., and Geldner, N. (2018). A protocol for combining fluorescent proteins with histological stains for diverse cell wall components. Plant J. *93*, 399–412.

Valeska Zeisler-Diehl, V., Migdal, B., and Schreiber, L. (2017). Quantitative characterization of cuticular barrier properties: methods, requirements, and problems. J. Exp. Bot. *68*, 5281–5291.

Van Norman, J.M., Xuan, W., Beeckman, T., and Benfey, P.N. (2013). To branch or not to branch: the role of pre-patterning in lateral root formation. Development *140*, 4301–4310.

Vermeer, J.E.M., von Wangenheim, D., Barberon, M., Lee, Y., Stelzer, E.H.K., Maizel, A., and Geldner, N. (2014). A spatial accommodation by neighboring cells is required for organ initiation in Arabidopsis. Science *343*, 178–183.

Vilches-Barro, A., and Maizel, A. (2015). Talking through walls: mechanisms of lateral root emergence in *Arabidopsis thaliana*. Curr. Opin. Plant Biol. *23*, 31–38.

Voß, U., Wilson, M.H., Kenobi, K., Gould, P.D., Robertson, F.C., Peer, W.A., Lucas, M., Swarup, K., Casimiro, I., Holman, T.J., et al. (2015). The circadian clock rephases during lateral root organ initiation in *Arabidopsis thaliana*. Nat. Commun. *6*, 7641.

Willemsen, V., Bauch, M., Bennett, T., Campilho, A., Wolkenfelt, H., Xu, J., Haseloff, J., and Scheres, B. (2008). The NAC domain transcription factors FEZ and SOMBRERO control the orientation of cell division plane in Arabidopsis root stem cells. Dev. Cell *15*, 913–922.

Xing, Q., Creff, A., Waters, A., Tanaka, H., Goodrich, J., and Ingram, G.C. (2013). ZHOUPI controls embryonic cuticle formation via a signalling pathway involving the subtilisin protease ABNORMAL LEAF-SHAPE1 and the receptor kinases GASSHO1 and GASSHO2. Development *140*, 770–779.

Yang, W., Pollard, M., Li-Beisson, Y., and Ohlrogge, J. (2016). Quantitative analysis of glycerol in dicarboxylic acid-rich cutins provides insights into Arabidopsis cutin structure. Phytochemistry *130*, 159–169.

Yeats, T.H., Huang, W., Chatterjee, S., Viart, H.M.F., Clausen, M.H., Stark, R.E., and Rose, J.K.C. (2014). Tomato Cutin Deficient 1 (CD1) and putative orthologs comprise an ancient family of cutin synthase-like (CUS) proteins that are conserved among land plants. Plant J. *77*, 667–675.

Zeisler-Diehl, V., Müller, Y., and Schreiber, L. (2018). Epicuticular wax on leaf cuticles does not establish the transpiration barrier, which is essentially formed by intracuticular wax. J. Plant Physiol. *227*, 66–74.

Zhu, J.-K. (2016). Abiotic stress signaling and responses in plants. Cell *167*, 313–324.

Ziv, C., Zhao, Z., Gao, Y.G., and Xia, Y. (2018). Multifunctional roles of plant cuticle during plant-pathogen interactions. Front. Plant Sci. *9*, 1088.

STAR★METHODS

KEY RESOURCES TABLE

REAGENT or RESOURCE	SOURCE	IDENTIFIER
Antibodies		
Monoclonal antibody to xylogalacturonan	Plantprobes	LM8
Anti-Rat IgG–FITC antibody produced in goat	Sigma-Aldrich	Cat#F6258; RRID: AB_259695
Chemicals, Peptides, and Recombinant Proteins		
Fluorol Yellow 088	Sigma-Aldrich	Cat#F5520
Aniline Blue diammonium salt	Sigma-Aldrich	Cat#415049
Toluidine Blue	Sigma-Aldrich	Cat#89640
Fluorescein diacetate	Sigma-Aldrich	Cat#F7378
ω-pentadecalacton	Sigma-Aldrich	Cat#W2840009
Methylheptadecanoate	Sigma-Aldrich	Cat#H4515
N, O- bis(trimethysilyl)-trifluoroacetamide with trimethylchlorosilane (BSTFA)	Sigma-Aldrich	Cat#15238
Pyridine	Sigma-Aldrich	Cat#270970
Methyl acetate	Sigma-Aldrich	Cat#296996
Sodium methoxide	Sigma-Aldrich	Cat#156256
Dichloromethane	Sigma-Aldrich	Cat#650463
Calcolfluor white (Fluorescent brightener 28)	Polysciences	Cat#4359
Xylitol	Sigma-Aldrich	Cat#X3375
Sodium deoxycholate	Sigma-Aldrich	Cat#30970
Urea	Sigma-Aldrich	Cat#51456
Potassium hexacyanoferrate(II) trihyadrate	Sigma-Aldrich	Cat#60280
Low viscosity Embedding media Spurr	EMS	Cat#14300
Osmium tetroxide 4%	EMS	Cat#19150
Experimental Models: Organisms/Strains		
Arabidopsis: gpat4	Li et al., 2007	SALK_106893
Arabidopsis: gpat8	Li et al., 2007	SALK_095122
Arabidopsis: gpat4 gpat8	Li et al., 2007	Cross between *gpat4* and *gpat8*
Arabidopsis: dcr-2	Panikashvili et al., 2009	SALK_128228
Arabidopsis: bdg-1	Kurdyukov et al., 2006	W32 mutant
Arabidopsis: gso1-1/sng3-1	Pfister et al., 2014	SALK_064029
Arabidopsis: gso2-1	Tsuwamoto et al., 2008	SALK_130637
Arabidopsis: gso1-1 gso2-1	Moussu et al., 2017	Cross between *gso1-1* and *gso2-1*
Arabidopsis: smb-3	Willemsen et al., 2008	SALK_143526
Arabidopsis: pLOVE1::CDEF1	This study	Transgenic Col-0
Arabidopsis: pGPAT4::NLS-GFP-GUS	This study	Transgenic Col-0
Arabidopsis: pGPAT8::NLS-GFP-GUS	This study	Transgenic Col-0
Arabidopsis: pDCR::NLS-GFP-GUS	This study	Transgenic Col-0
Arabidopsis: pBDG::GFP	Jakobson et al., 2016	Transgenic Col-0
Oligonucleotides		
For all oligonucleotides used for genotyping and cloning	See Table S1B	N/A
Recombinant DNA		
All recombinant DNA needed for the generation of transgenic lines are described in the subsection of the Method Details- Generation of constructs	This paper	N/A

(*Continued on next page*)

Continued

REAGENT or RESOURCE	SOURCE	IDENTIFIER
Software and Algorithms		
Fiji	Schindelin et al., 2012	https://fiji.sc/#; RRID: SCR_002285
Rstudio	RStudio Team, 2015	https://www.rstudio.com/; RRID: SCR_000432

CONTACT FOR REAGENT AND RESOURCE SHARING

Further information and requests for resources and reagents should be directed to and will be fulfilled by the Lead contact Christiane Nawrath (christiane.nawrath@unil.ch).

EXPERIMENTAL MODEL AND SUBJECT DETAILS

Plant material

Arabidopsis thaliana accession Col-0 was used in this work along with *Brassica nigra* and *Solanum lycopersicum* L. "Moneymaker." All *Arabidopsis* seeds were maximally 3-month-old for the characterization of the RCC.

Arabidopsis thaliana mutants were already described: *gpat4, gpat8, gpat4 gpat8* (Li et al., 2007), *dcr-2* (Panikashvili et al., 2009), *bdg-1* (Kurdyukov et al., 2006), *smb-3* (Willemsen et al., 2008), *gso1/sng3-3* (Pfister et al., 2014), *gso2-1* (Tsuwamoto et al., 2008) and *gso1/sng3-3 gso2-1* (Moussu et al., 2017). Gene numbers and genotyping primers are described in Tables S1A and S1B.

Growth conditions

For the characterization of the RCC plants were grown under sterile conditions. Seeds were surface sterilized with chlorine gas. After 2-3 days of vernalization at 4°C, plants were grown on ½ MS (Murashige and Skoog, 500mg/l MES, pH 5.7), 0.7% agar at 22°C, under continuous light (100 μmol m^{-2} s^{-1}). With the exception of the seedlings for polyester extraction and salt stress assays, plants were grown vertically. For transformation and seed amplification plants were grown on soil under continuous light (100 μmol m^{-2} s^{-1}) at 20°C and 65% humidity.

METHOD DETAILS

Generation of constructs

To generate pENTRY L4-pGPAT4-R1 and pENTRY L4-pGPAT8-R1, 1.7 kb and 2.2 kb fragments upstream of each *GPAT* were amplified, respectively, and cloned into pDONR P4-P1 using KpnI and XbaI restriction site. pENTRY L4-pLOVE1-R1 was generated by amplifying a 2.1 kb fragment upstream of *LOVE1* and recombining it into pDONR P4-P1. To generate pENTRY-L1-NLS-GFP-GUS-L2, *NLS-GFP-GUS* was amplified from a pDEST containing B1-NLS-GFP-B2-GUS-B3 and recombined into pDONR221. All primers used are shown in Table S1B. pENTRY L1-CDEF1-L2 was previously described (Naseer et al., 2012). pGPAT4::NLS-GFP-GUS, pGPAT8::NLS-GFP-GUS and pLOVE1::CDEF1 were generated by recombining the corresponding entry clones into the pMMA-Red vector (Ali et al., 2012) using the Gateway Technology (Lifesciences). pLOVE1::H2A-GFP was generated by recombining pENTRY-L4-pLOVE1-R1 and pENL1-GAL4-VP16-L2 into the destination vector pB9-H2A-UAS-7m24GW. This vector contains a HISTONE 2A-6 (H2A) coding sequence (At5g59870) fused to eGFP and driven by the repetitive UAS promoter (Olvera-Carrillo et al., 2015). pBDG::GFP was previously described (Jakobson et al., 2016). All constructs were transformed in *Agrobacterium tumefaciens* and then in *Arabidopsis thaliana* accession Col-0 using the floral dip method (Clough and Bent, 1998): inflorescences were dipped into a 5% sucrose/0.05% Silwet L-77 solution containing *Agrobacterium* for 2-3 s and kept at high humidity for 24 h. Transformed seeds were selected based on their red fluorescence (Ali et al., 2012).

Cutin digestion, cuticle staining and permeability assays

The polyester of the RCC was digested *in vitro* by a recombinant cutinase (Unilever). Samples were fixed in acetone 90% for 30 min at −20°C, washed several time in 0.2M K_2HPO_4 pH8 and placed in a tube with 100 μg/ml cutinase in 0.2M K_2HPO_4 pH8 for three days, the negative control plants were incubated in 0.2M K_2HPO_4 without cutinase.

The polyester of the RCC of primary roots was specifically digested *in vivo* in transgenic pLOVE1::CDEF1 lines. In order to evaluate whether the pLOVE1 promoter was suitable to express a cutinase specifically in the outer root cap cell layer its activity was evaluated in several independent pLOVE1::H2A-GFP lines (Figure S4A). Furthermore, several independent transgenic pLOVE1::CDEF1 lines were investigated for giving consistent results in respect to the RCC degradation (Figure S4B).

For visualization of cell wall polyesters, the Fluorol Yellow 088 protocol from Naseer et al. (2012) was modified to remove background staining in lipid-rich organs and validated (Figure S4C). Shortly, seedlings were incubated in Fluorol Yellow 088

(0.01% in methanol) during 3 days for investigations of roots and for three weeks for aerial parts of the plants. Specimen were then counterstained with aniline blue (0.5% in water) for minimum 1 h at RT and rinsed in water. 10 roots each were studied in three independent experiments.

For studying the permeability of the RCC with toluidine blue, 10-12 roots were harvested in 0.5 x liquid MS medium and then simultaneously incubated in an aqueous solution of 0.05% toluidine blue/0.1% Tween 20 during the indicated time (10-135 s) followed by a quick washing step in water. Samples were instantaneously evaluated under the Axio Zoom V16 microscope (Zeiss) coupled to an Axiocam 512 Color camera for the presence or absence of dark-blue staining of the meristematic cells (Figure S4D). A staining of the mucilage at the columella (Figure S2) was present at all times in WT and mutants (Figure S4C). The experiment was repeated three times.

For studying the permeability of the cuticle with fluorescein diacetate (FDA) (5 μg/ml in ½ MS) (Barberon et al., 2016), 25 lateral roots of the same developmental stage originating from 3 independent experiments were individually investigated by direct application of FDA to the root on the microscope slide, immediately mounted and observed as described below. The same microscope and same settings were used for the analysis and a 4-min incubation period was selected for comparison of the different genotypes. The Fire scale of relative intensity was used for the comparison (Schindelin et al., 2012).

Germination and root growth assays

Salt stress assays were conducted by placing seeds on medium containing 75 mM of K_2SO_4, 250 mM of mannitol, 100 mM of KCl or 100 mM of NaCl, respectively. Four replicates were evaluated for each treatment (50-100 seeds each) and 3 for controls. Experiments were repeated independently three times and a representative dataset is presented. Salt concentrations had been optimized to minimize the effects on plant development of WT by using 50-200 mM of K_2SO_4, 200-400 mM of mannitol, 100-200 mM of KCl or 100-200 mM of NaCl.

NaCl-induced cell death assay was conducted by incubating of 2-day-old seedlings in ½ MS medium containing 140 mM NaCl for 10 min. Seedlings were subsequently treated for 10 s with propidium iodide (PI) (10 μg/mL) and immediately observed under the microscope (Olvera-Carrillo et al., 2015). The number of dead cells was determined by counting the cells fully stained by PI in the entire meristem using a z-stack of pictures. 16-20 meristems were observed per genotype. Experiments were repeated independently two times and a representative dataset is presented.

Lateral root emergence was induced on 5-day-old seedlings by turning the plate of 90°C (Voß et al., 2015). Stages of lateral root emergence were evaluated after 42 h or 96 h, using mutant roots having a comparable length to WT. Roots were fixed and cleared by the following incubation steps: 4% HCl/20% methanol solution for 15 min at 57°C, 7% NaCl/60% ethanol solution for 15 min at RT, rehydrated by 10 min incubation in 60%, 40%, 20%, 10% ethanol. Specimens were mounted in 50% glycerol/5% ethanol and stages of lateral root emergence were determined using a Leica DM5000B microscope (Malamy and Benfey, 1997). Experiments were repeated independently three times (n = 20-30) and a representative dataset is presented.

To study the shape of lateral root primordia seedlings were fixed, cleared and stained with Calcofluor as described in Ursache et al. (2018). Briefly, the seedling was fixed in 4% paraformaldehyde for 1 h, then washed twice in 1x PBS and cleared overnight in Clearsee (10% Xylitol/15% Sodium deoxycholate/25% Urea). Afterward the specimens were staining in 0.1% Calcofluor white in Clearsee for 1 h and washed in Clearsee for max 30 min before being imaged, as described below. Adhesion frequency was assessed by studying 90 - 160 seedlings of each genotype at the early observation time (42 h and 48 h) and approximately 100 seedlings at the late observation time (96 h).

Immunofluorescence labeling

To label mucilage, the protocol of Durand et al. (2009) was used to detect xylogalacturonan-associated epitopes with the LM8 antibody, which was revealed with a fluorescein isothiocyanate (FITC)-conjugated goat anti-rat antibody. Briefly, 2-day-old seedlings were fixed for 30 min in 4% paraformaldehyde/1% glutaraldehyde/50 mM PIPES pH 7.0/1 mM $CaCl_2$ and washed in 50 mM PIPES pH 7.0 with 1 mM $CaCl_2$. After a 30 min incubation in 3% low-fat milk/PBS (phosphate-buffered saline) pH 7.2 as blocking solution, seedlings were washed in 0.05% Tween 20 (PBST) and incubated overnight with the LM8 antibody (1:5 in 0.1%PBST) at 4°C. Samples were then washed 5 times in 0.01% PBST and incubated for 2 h at 28°C in FITC-conjugated goat anti-rat as secondary antibody (1:50 in 0.1% PBST). A minimum of 30 roots of each genotype was studied.

Fluorescence Microscopy

Most fluorescent microscopy studies were performed on the confocal laser-scanning microscope ZEISS 700 with an excitation at 488 nm and detection with BP 490-555 nm for GFP, FY, FDA and LM8, and respectively at 555 nm and LP 640 nm for PI. PI (10 μg/mL) was used for staining the cell wall of the roots during the study of gene expression by direct application on the slide. Calcofluor staining was studied on the confocal ZEISS LSM 880 Airyscan with an excitation at 405 nm and detection at 425-475 nm. Red seeds selection was performed under the stereomicroscope Leica 6000 equipped with a DSR filter.

Transmission electron microscopy

The protocol for transmission electron microscopy of Barberon et al. (2016) was slightly modified. Roots were fixed in a 2.5% glutaraldehyde solution in 0.1 M phosphate buffer pH 7.4 (PB) for 1 h at RT followed by a postfixation (1 h at RT) in a freshly made solution of

1% osmium tetroxide and 1.5% potassium ferrocyanide in PB and then washed in distilled water. Dehydration steps were then gradually performed in ethanol solution (30%, 50%, 70% for each 40 min, 100% twice for 1 h). The infiltration with Spurr resin at 33% in ethanol for 4 h, 66% for 4 h and 100% for 8 h twice was achieved before polymerization at 60°C for 48 h. Root tips were cut longitudinally in ultrathin sections of 50 nm of thickness and studied with a FEI CM100 transmission electron microscope (FEI, Eindhoven, the Netherlands) coupled with a TVIPS TemCamF416 digital camera (TVIPS GmbH, Gauting, Germany) (acceleration voltage of 80 kV). The ultrastructure of the root cap cell wall and cuticle was investigated over the entire length of the root cap in 2-3 independent root tip preparations per genotype and representative pictures were taken. Cuticle thickness was determined by taking 4 pictures per root and 5 measurements per picture for 5 primary roots and 3 lateral roots at a magnification of 20.000 (0.5101 nm/pixel). The ultrastructure of the RCC at the emerging LR was investigated at the stage when the lateral root had just emerged from the primary root and thus its exact position could be identified by light microscopy.

Chemical analyses

The protocol for the determination of ester-bond lipids previously described in Barberon et al. (2016) was adapted. 200 mg of seeds were grown on nylon mesh (200 μm pore size). After two days, the roots were shaved off after flash freezing and extracted in isopropanol/0.01% butylated hydroxytoluene (BHT). They were then delipidized three times (1 h, 16 h, 8 h) in each of the following solvents, i.e., chloroform-methanol (2:1), chloroform-methanol (1:1), methanol with 0.01% BHT, under agitation before being dried for 3 days under vacuum. Depolymerization was performed by base catalysis (Li-Beisson et al., 2013). Briefly, dried plant samples were transesterified in 2 mL of reaction medium. 20 mL reaction medium was composed of 3 mL methyl acetate, 5 mL of 25% sodium methoxide in dry methanol and 12 mL dry methanol. The equivalents of 5 μg of methyl heptadecanoate and 10 μg of ω-pentadecalactone/sample were added as internal standards. After incubation of the samples at 60°C for 2 h 3.5 mL dichloromethane, 0.7 mL glacial acetic acid and 1 mL 0.9% NaCl (w/v) Tris 100 mM pH 8.0 were added to each sample and subsequently vortexed for 20 s. After centrifugation (1500 g for 2 min), the organic phase was collected, washed with 2 mL of 0.9% NaCl, and dried over sodium sulfate. The organic phase was then recovered and concentrated under a stream of nitrogen. The resulting cutin monomer fraction was derivatized with BFTSA/pyridine (1:1) at 70°C for 1 h and injected out of hexane on a HP-5MS column (J&W Scientific) in a gas chromatograph coupled to a mass spectrometer and a flame ionization detector (Agilent 6890N GC Network systems). The temperature cycle of the oven was the following: 2 min at 50°C, increment of 20°C/min to 160°C, of 2°C/min to 250°C and 10°C/min to 310°C, held for 15 min. 3 independent experiments were performed with 3-4 replicates for each genotype, respectively, and a representative dataset is presented. The amounts of unsubstituted C16 and C18 fatty acids were not evaluated because of their omnipresence in the plant and in the environment.

QUANTIFICATION AND STATISTICAL ANALYSIS

For the germination assay, the cell death assay and the chemical analyses of the cutin composition, presented values are the mean ± standard deviation. Student's t-test analyses were performed to highlight differences between WT and other genotypes. Asterisks illustrate the p value: $p < 0.001$ is ***, $p < 0.01$ is ** and $p < 0.05$ is *.

Number of repetitions and replicates are mentioned for each experiment in the METHOD DETAILS.

Cell

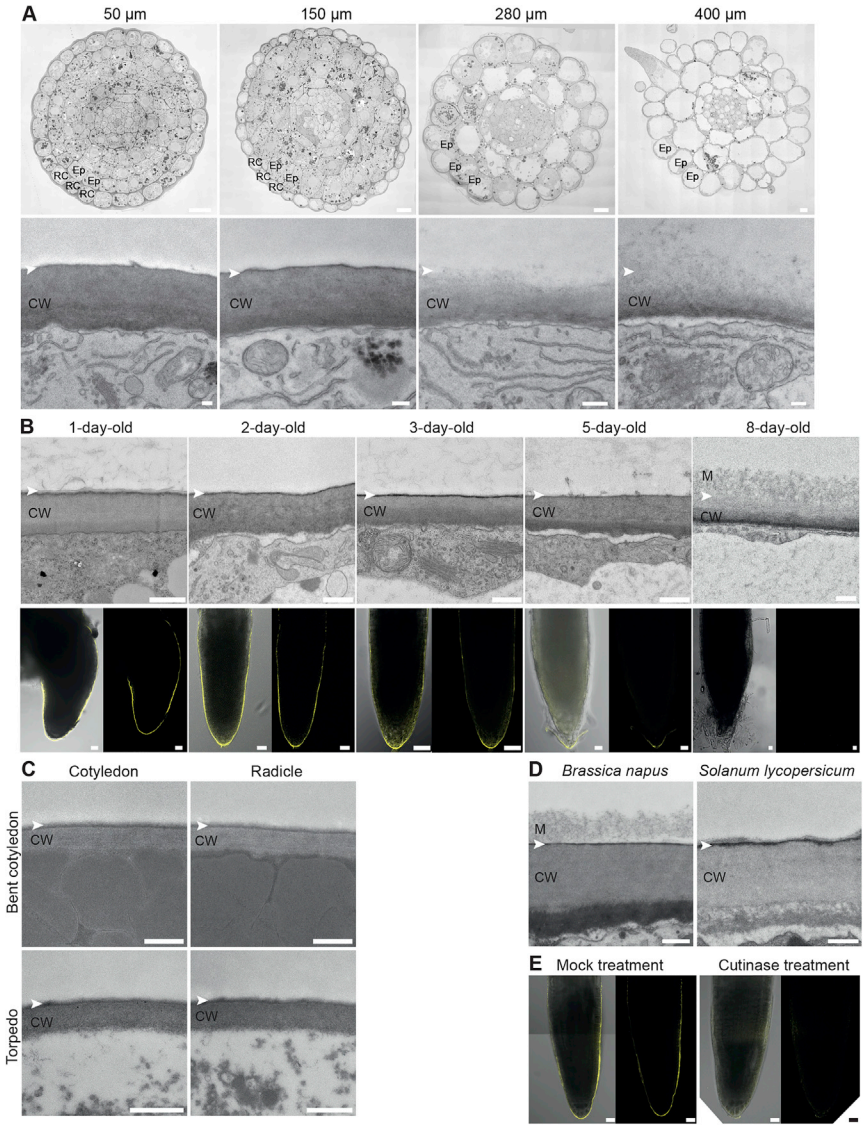

Figure S1. RCC of the Primary Root of *Arabidopsis* and Other Plant Species and Its Degradation by Cutinase *In Vitro*, Related to Figure 1B

(A) Transversal root sections at the indicated distance from the extremity of the root tip of a 2-day-old WT seedling, as visualized by TEM (top) and zoom to the outer cell wall of the outermost cell layer (bottom). At 50 and 150 µm, lateral root cap cells form the outermost cell layer of the root tip having an electron-opaque layer at the surface of the outer cell wall. At 280 and 400 µm, epidermal cells form the outermost cell layer having no electron-opaque layer. The scale bars in the overview represent 10 µm and in the zoom 200 nm. Overview pictures are stitched together from multiple TEM pictures.

(B) TEM pictures of root tips of WT showing cell wall and cuticle of the outermost lateral root cap cells (top) and median views of the FY staining at the root cap at indicated ages (bottom; on the left, overlay bright field and fluorescence; on the right, fluorescence only). With the loss of the first root cap cells, the RCC is not present anymore. Scale bars in TEM pictures represent 500 nm and in fluorescence micrographs 20 µm.

(C) Cell wall and cuticle ultrastructure of embryonic organs at torpedo and bent cotyledon stage, as visualized by TEM. Scale bars represent 500 nm.

(D) Lateral root cap cells of 2-day-old seedlings of *Brassica napus* and *Solanum lycopersicum,* both having an electron-opaque layer at the outside of the primary cell wall in TEM. Scale bars represent 500 nm.

(E) Median views of FY staining of the tips of 2-day-old roots treated with recombinant cutinase and respective controls showing the absence of the RCC after cutinase treatment. Scale bars represent 20 µm.

CW, cell wall; Ep, epidermal cell; M, mucilage; RC, root cap cell; white arrow head, expected position of the RCC.

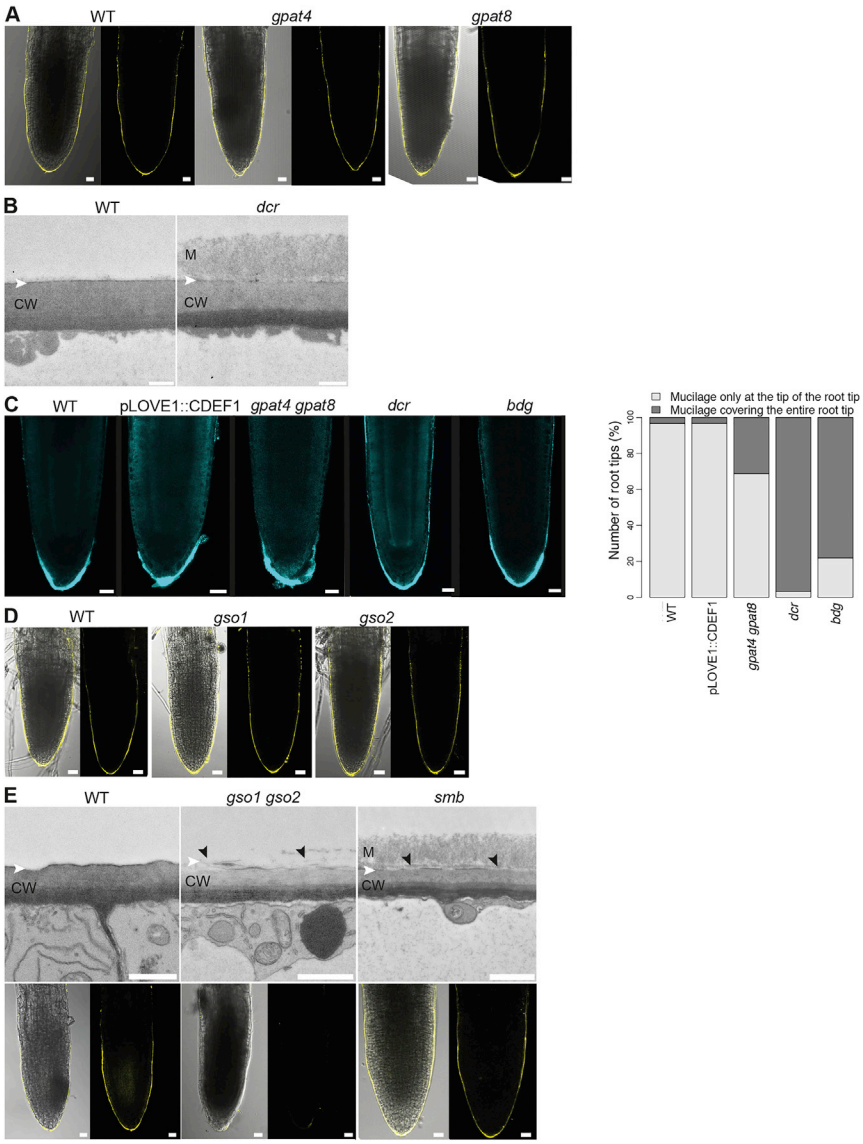

Figure S2. Characterization of the RCC and Other Cell Wall Structures in Different Genotypes, Related to Figure 1E

(A) Median views of FY staining at the RCC of the primary root of 2-day-old *gpat4* and *gpat8* mutants in comparison to WT (on the left, overlay bright field and fluorescence; on the right, fluorescence only). Scale bars represent 20 μm.

(B) Ultrastructure of cell wall and cuticle of lateral root cap cells of 2-day-old root after a 3-day-long methanol-treatment. Although the ultrastructure of the cell wall is not largely altered in WT, in *dcr* mutant, globular electron-opaque depositions in the cell wall and at the cell wall-mucilage interface visible without methanol treatment (Figure 1E) were not present anymore. Scale bar represents 500 nm.

(C) Mucilage deposition at the root cap of 2-day-old seedlings as assessed by immunolabelling with the LM8 antibody detecting xylogalacturonan-associated epitopes of *Arabidopsis* root caps (Durand et al., 2009). Quantitative evaluation of mucilage localization in the observed root tips is shown on the right of representative picture. Scale bars represent 20 μm.

(D) Median view of FY staining of the RCC of the primary root of *gso1* and *gso2* in comparison to WT (on the left, overlay bright field and fluorescence; on the right, fluorescence only). Scale bars represent 20 μm.

(E) Alterations in the cell wall and cuticle ultrastructure of the outermost lateral root cap cells (top) and median views of the FY staining at the root cap (bottom; on the left, overlay bright field and fluorescence; on the right, fluorescence only) of WT, *gso1 gso2* mutant having no RCC and *smb* mutant having an interrupted RCC. Scale bars in TEM pictures represent 500 nm and in pictures showing FY staining 20 μm.

CW, cell wall; M, mucilage; black arrowhead, interruption of the cuticle; white arrowhead, expected position of the RCC.

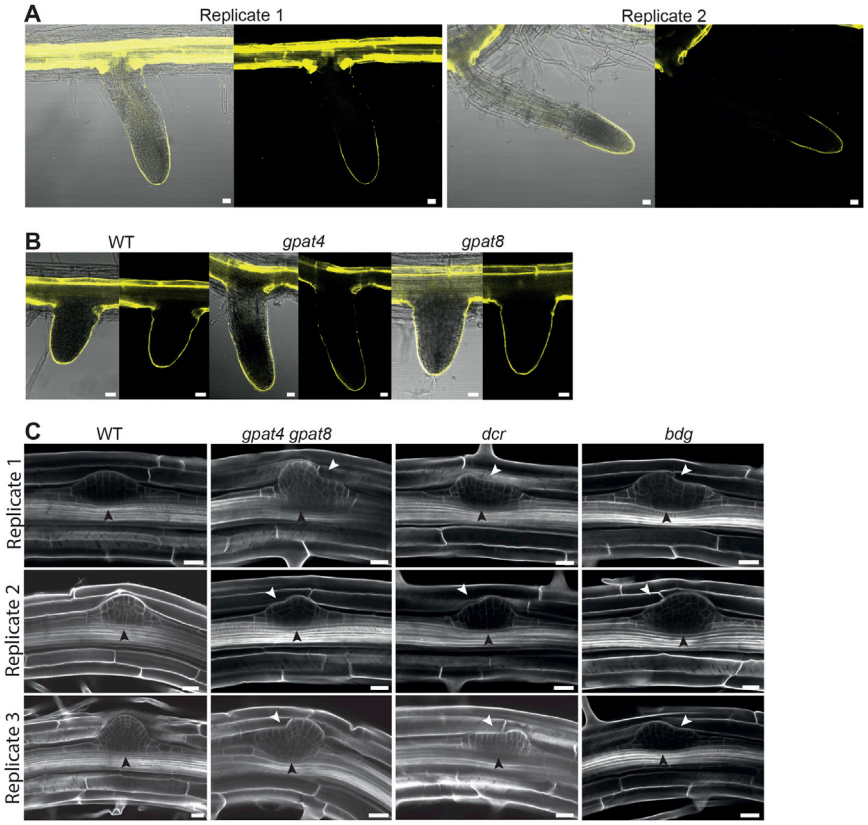

Figure S3. The RCC of the Lateral Root and Its Role in Lateral Root Emergence, Related to Figures 3D, 4D, and 4E

Median views of FY staining in 8-day-old WT seedlings (A) at the RCC of lateral roots having different lengths and (B) at the RCC of shortly-emerged lateral roots of *gpat4* and *gpat8* in comparison to WT (left, overlay bright field and fluorescence; right, fluorescence only). As expected, the suberin of the endodermis is also stained. Scale bars represent 20 μm.

(C) Shape of lateral root primordia in WT and different genotypes having a modified RCC at the emerging lateral root. Regular shape of lateral root primordia of WT. Deformed lateral root primordia of genotypes having RCC modifications at the lateral root primordium. Black arrowhead, lateral root primordium; white arrowhead, primordium deformation. Scale bars represent 20 μm.

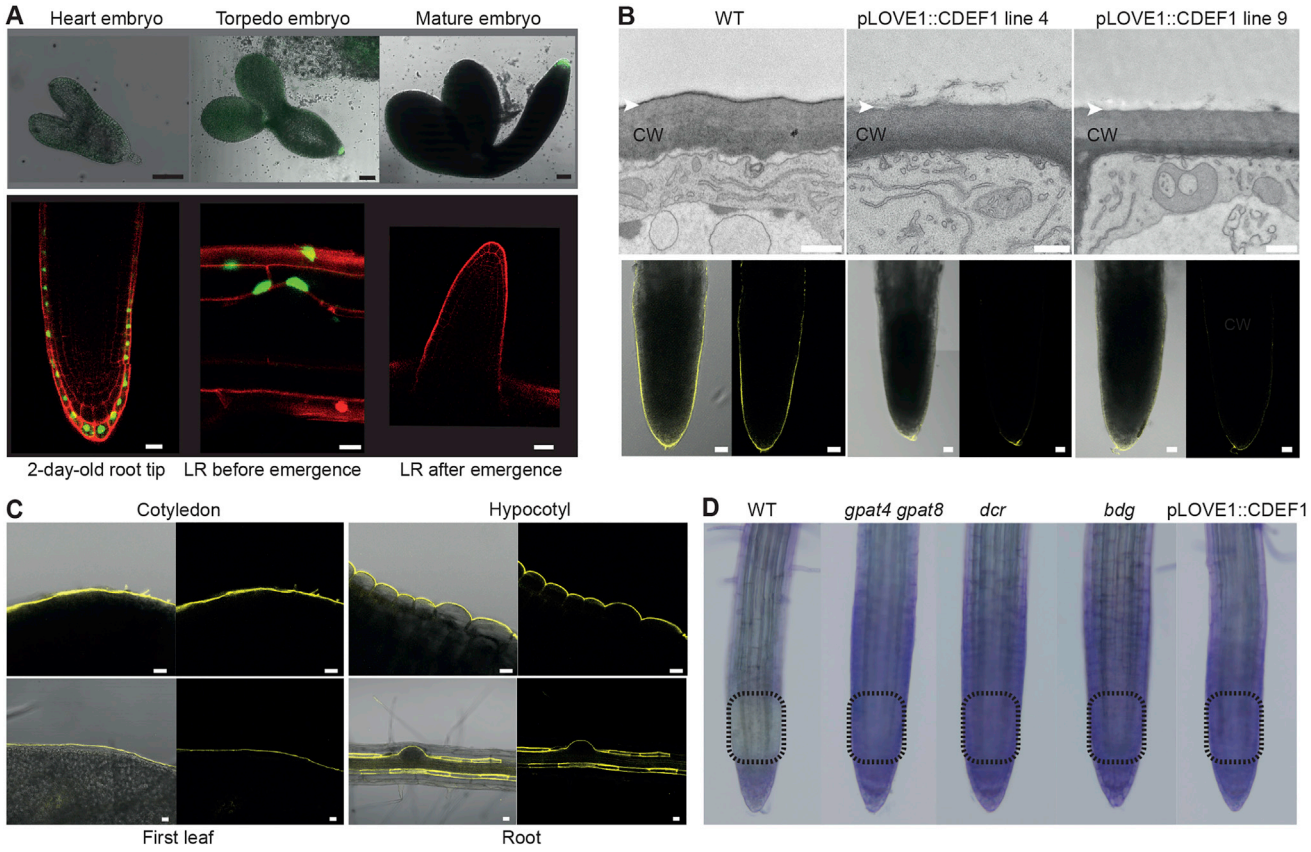

Figure S4. Generation of pLOVE1::CDEF1 Plants, Fluorol Yellow and Toluidine Blue Staining, Related to STAR Methods

(A) Activity of pLOVE1 was assessed in different organs and at different developmental stages in transgenic *Arabidopsis* lines expressing pLOVE1::H2A-GFP. Scale bars represent 50 μm (top row) and 20 μm (bottom row).

(B) Ultrastructure of cell wall and cuticle of the outermost lateral root cap cells as visualized by TEM (top) and median views of the FY staining at the root cap of WT and different transgenic lines expressing pLOVE1::CDEF1 having no RCC (bottom: on the left, overlay bright field and fluorescence; on the right, fluorescence only). Scale bars represent 500 nm (top) and 20 μM (bottom). CW, cell wall; white arrowhead, expected position of RCC. pLOVE1::CDEF1 line 4 has been selected to be shown as representative pLOVE1::CDEF1 line in Figure 1B together with its WT control.

(C) Various organs of 8-day-old WT seedlings were stained with FY using the modified staining protocol showing that cutin and suberin can be stained. Scale bars represent 20 μm.

(D) Toluidine blue staining of the primary root of 2-day-old seedlings of WT and different genotypes having RCC modifications after 30 s of incubation. The staining at the extremity of the root tip is due to the mucilage at the columella cells (See Figure S2C) that also stains with toluidine blue. Dashed box; zone of evaluation.